2025 SPE/IADC International Drilling Conference and Exhibition

SPE-223715

Bit-Rock Interaction for PDC Drill Bits: A Review and an Open-Source Library

E. Ghaly [1]*, and R. J. Shor [1]

[1]Harold Vance Department of Petroleum Engineering, Texas A&M University, College Station, Texas, United States

Abstract

The polycrystalline diamond compact (PDC) bit is the most used bit type in deep drilling with a global market worth over $3.13 billion USD in 2023. Numerous models, ranging in complexity from a simple linear equation to fully coupled computational fluid dynamics discrete element method models, have been proposed in literature, yet no open-source implementation exists that includes a choice of fidelity and complexity. In this paper, we review the existing bit-rock interaction models, summarizing assumptions, construction methodology, validation data, prediction capabilities, and performance. A Python library of bit-rock models is also detailed and published via the Open-Source Drilling Community. An extensive literature review of published models starting from 1985 through today is conducted. Models ranging from single cutter models to full bit models are considered. High fidelity coupled finite element models constructed for specific geologic environments are included with the benefits and limitations of using this approach are discussed. The focus of the study is generalized physics-based models which can be coupled with a drillstring model to provide general performance guidelines. Model formulations, assumptions, limitations, and available validation are systematically presented to establish a clear understanding of the study's framework. The selected models, implemented in Python, are compared with downhole data across several scenarios. A workflow is then proposed to couple open source drillstring models with bit models, emphasizing the critical aspect of timestep synchronization. The bit models primarily describe the forces between the bit face and rock, considering the underlying physics of the drilling process. Additionally, current gaps in knowledge are highlighted to encourage future research and development in this domain.

Introduction

Diamond bit technology was first introduced in the United States when a prototype was field tested in November 1973. It showed promising performance but failed to establish a market due to its high cost and manufacturing problems (Offenbacher et al. 1983). It was reintroduced to the industry and successfully drilled soft formations and evaporites at the North Sea (Powell et al. 1980) & (Paterson 1982), carbonates and evaporites with water-based mud in the Middle East (Prooyen et al. 1982) and in Texas (Offenbacher et al. 1983). In particular, PDC bits demonstrated their reliability through a series of successes in Oklahoma while drilling through abrasive environment at high pressure and temperature, an environment where roller cone bits that showed repeated failures (Offenbacher et al. 1983).

The potential to eliminate a common failure mode of roller cone bits, bearing damage and failure, led to the continued development of PDC bits. Early commercial bits were diamond core bits and bits running with high-speed turbines. These bits were useful in small diameter holes and for milling through hard formations. However, uptake was limited due to high manufacturing cost as commercial grade of diamond was used. A variety of designs were used depending on the formation being drilled, thus mass production was limited as each bit was highly customized. The advent of synthetic diamond manufacturing in the early 1980s was a breakthrough which significantly reduced costs, improved the availability of PDC bits and accelerated adoption. Higher weight on bit (WOB) could be applied to these new PDC bits and longer run life began to be demonstrated. It was also observed that higher speeds could be reached safely. Shortly after their introduction, it was found that they perform better with oil base mud, however, the same performance can be attained with water base mud but with applying high flowrates (Millheim 1986).

After realizing the advantages of PDC bits over the roller cone bits, researchers and manufacturers began to optimize bit performance, either by optimizing the operating conditions or by improving the PDC bit design. Researchers focused their studies on understanding the PDC bit rock interactions and conducted experiments to define the optimum operating conditions. Most of the early studies included mapping the variation of applied parameters and developed empirical correlations, typically limited to a specific location and condition. These early empirical correlations were of limited use and only addressed a narrow scope of the whole PDC bit rock interactions.

Fig. 1 shows a typical PDC bit with its

This paper reviews the evolution in the understanding of PDC bit-rock interaction, from initial experiments to modern coupled bit simulation. First, early work in developing empirical correlations based on experimental tests, where the relationship is quantified between different parameters, is quantified. Next, the pioneering manufacturing breakthroughs which enabled the mass market adoption of PDC bits are summarized. Full 3D bit models are next presented with their objectives, methodology and validation. Afterwards, reduced mathematical models which simplify aspects of bit-rock interaction are presented, both for single cutters and for full bits, along with their formulation assumptions and limitations. Finally, an open-source Python library is presented for selected full bit models and compared with field data.

Empirical correlation

In 1986, Black et al. conducted experiments to study PDC bit performance. They found that the resultant rate of penetration (ROP) from those bits increased as the rotational speed increased at constant WOB. They tried four different values for WOB and acquired the same results noting that they recorded less ROP when increasing the rotational speed at elevated WOB due to the lack in hole cleaning. They conducted many experiments during their study and concluded that (Black et al. 1986):

1. After exceeding a threshold WOB, the penetration started and the WOB is directly proportional to the ROP
2. Increasing WOB and rotational speed would result in higher ROP, however, if the flow rate was not sufficient to clean the hole, an adverse effect was observed, and the ROP dropped
3. The increase in WOB was directly related to an increase in torque (TOB)
4. ROP increased linearly with increasing the mechanical horsepower at the bit

The previous observation can be sampled as seen in Error! Reference source not found. (Black et al. 1986).

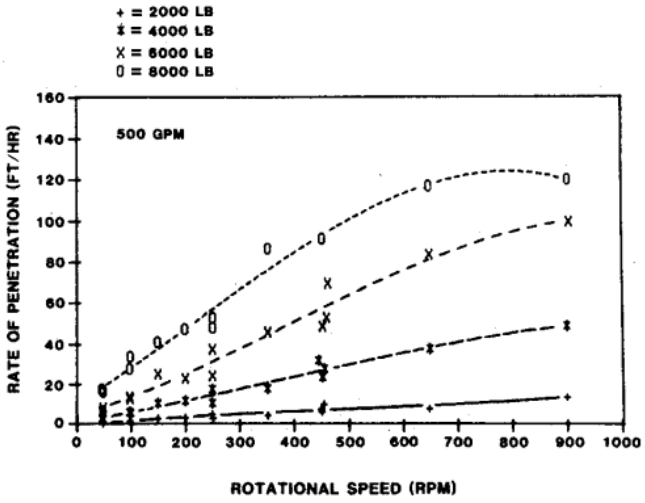

Figure 1: Black et al. empirical correlation example (Black et al. 1986)

In 1989, Glowka developed a model for PDC cutting process in high temperature and hard formations to determine the drag forces on each cutter. He conducted a series of experiments to study the forces required by a cutter to remove rock under various conditions and proposed the following relationship (Glowka 1989):

$$\frac{F}{A_w} = CD^n \tag{1}$$

Where F is the cutter penetration force, A_w is cutter area in contact with the rock, D is the cut depth, and C and n are fitting constants determined by the curve of best fit to the data by least square technique on log-log scale. He concluded that the penetration force is proportional to the cutter area in contact with the rock. He also noted that the penetrating forces were reduced greatly when he shifted from dry cutting conditions to jetting cutting conditions. Some of Glowka finds are seen in Error! Reference source not found. (Glowka 1989).

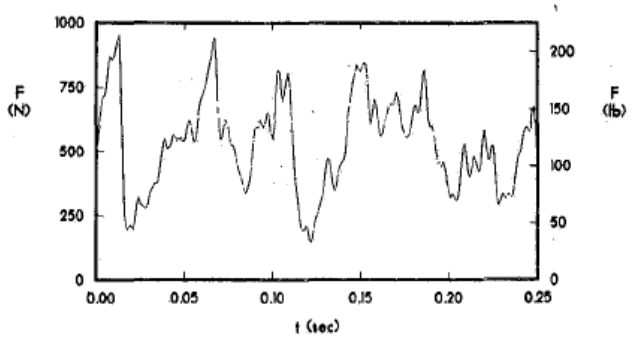

Figure 2: Glowka observations (Glowka 1989)

Warren and Armagost conducted similar experiments as Black et al., but on different formations, lower rotational speeds and a wider range of PDC bit designs from different manufacturers (Warren and Armagost 1988). Example of their work can be seen in **Figure 3**. Feenstra (1988) demonstrated that the primary advantage of PDC bits lies in their ability to drill more efficiently with reduced weight on bit (WOB). He also observed that tungsten carbide wears at least an order of magnitude faster than diamond, leaving the diamond layer to bear the full load (Feenstra 1988, Huang and Iversen 1981). Additionally, rock failure through shearing requires less energy compared to fracturing or crushing(Huang and Iversen 1981). Feenstra also observed that the self-sharpening nature of the cutters enhances their performance and recommended bit design improvements, such as directing cuttings away from the bit face and incorporating side rakes. These recommendations are consistent with the findings of Huang and Iversen(Huang and Iversen 1981), who concluded that increasing the side rake angle can mitigate bit balling when hydraulics are insufficient by enhancing the side force applied to the cuttings.

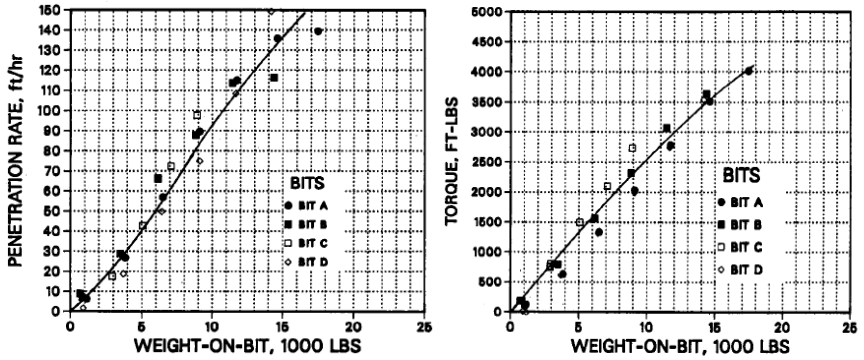

Figure 3: Examples of Warren and Armagost observations (Warren and Armagost 1988)

In 1988, Sneddon and Hall studied PDC bits failure by exploring the two materials separately: the polycrystalline diamond layer and tungsten carbide with cobalt, with the aim of defining each material's failure mode (Sneddon and Hall 1988). Andersen and Azar studied the effect of pressure on rock shearing and found that with the increase in the confining pressures, ROP dropped significantly (Andersen and Azar 1993). They attributed this phenomenon to bit balling and the higher specific energy required to fail the rock. A new hypothesis was introduced to the industry in 1993 by Smith et al.: the build-up-edge theory which basically suggests that during the cutting of ductile materials, a small amount of material adheres to the leading edge of the cutter rather than being removed with the chip. This phenomenon increases friction and makes the cutter behave as though it is dull. In rock drilling, this theory is used to explain the formation of a BUE at the cutter tip, which can reduce cutting efficiency and increase specific energy requirements (Smith et al. 1995). They proposed to decrease or prevent bit balling by modifying the cutting body to achieve perfect shearing, thus preventing cuttings stacking. This reduced the friction coefficient of cutters, leading to lower axial and tangential loads necessary to fail rock while maintaining ROP.

To improve bit body design, Mensa-Wilmot and Penrose stated that for applying the PDC bits in hard abrasive formations it must have maximized axial and radial diamond volume. They designed a new bit according to their theory with cutters at varied back rake angles in a way to cover the whole wellbore. They made lab and field studies proving that their new bit design was more reliable and suitable for hard abrasive formations (Mensa-Wilmot and Penrose 2003).

While these studies helped define suitable operating conditions and proved the importance of PDC bits, these studies did not establish a complete physical understanding of the PDC bit-rock interaction. The next sections detail first the manufacturing breakthroughs that improved reliability of PDC bits and then review the different approaches and simulation techniques utilized to understand the physics of bit-rock interaction, ranging from a single cutter to a full 3D coupled fluid-mechanical representation.

Manufacturing breakthroughs

Industry focused on enhancing the PDC bit performance through improvements in design and material. We highlight several key improvements which allowed for ROP increases. In 2002, a low friction fluoropolymer-based coating was developed that increased the ROP by factor of 5 while reducing the axial and tangential forces by 25% and 15% respectively (Mat et al. 2002). Improved coating formulations were announced in 2015, based on improving the fluoropolymer-based one to improve their durability. ROP enhancements of up to 40% were announced with 70% improvements in footage, as presented in **Figure 4** (Radford et al. 2015).

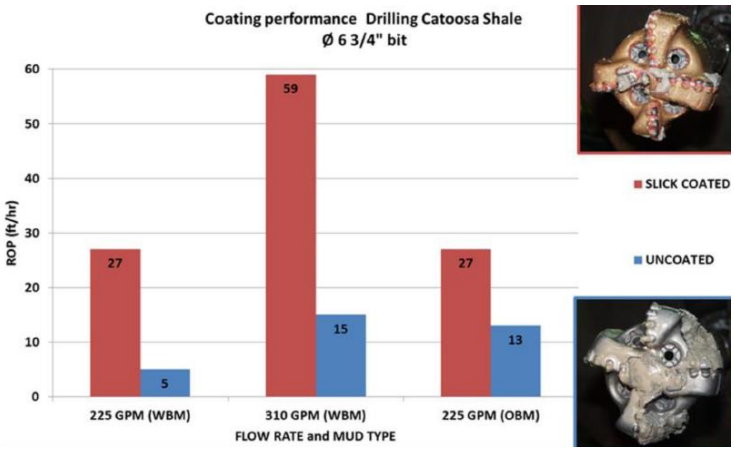

Figure 4: Radford et al. results (Radford et al. 2015)

Radtke et al. improved the TSP cutters by modifying the manufacturing process through using microwave heating or combustion synthesis or combination of both and it succeeded to improve those cutter fracture and impact resistance (Radtke et al. 2004). Other authors took another track. It started to improve the cutter geometrical shape. They succeeded to manufacture a bit body with one order of magnitude lower resistance to wear resulting in increasing the bit life by 30% longer than near offsets (Yazidi 2013). In 2020, another breakthrough was made. A new ultra-high pressure and high temperature device was invented that can produce polycrystalline diamond compact with totally free cobalt catalyst in the diamond structure (Zhan et al. 2020). Authors succeeded in maximizing the cutter thermal stability. When compared with the normal PDC cutters, it was found that the new cutters exhibit more than 200% higher fracture toughness and wear resistance (Zhan et al. 2020).

Full 3D bit models

Improvements in computing power in the 1980s and 1990s allowed for fully realized three dimensional realizations of PDC bits to be modelled to explore rock failure and fluid dynamics. These models are constructed using FEM or DEM using various software packages and allowed full bit behavior to be explored in a specific geological setting. However, these models are fit for purpose and require extensive data to represent the rock and bit meshes to ensure reliable results. Application of model results are frequently not generalizable and are frequently computationally intensive.

In early 1985, Baird et al. devised 3D bit simulator as a part of their full 3D drillstring simulator. Their aim was to capture the effect of PDC bit on the drillstring performance. However, this model had a major assumption where the rock removal at the bit-rock interface was not considered (Baird et al. 1985). Langeveld considered the assumption of Baird and concentrated also on bit dynamics. However, he only considered the cylindrical cutter (Langeveld 1992).

In 1993, Behr et al. constructed a 3D model for the PDC bits to simulate the real drilling conditions surrounding the bit attempting to capture the effect of bit whirl and drilling nonhomogeneous rocks. They mentioned that all the previous models assumed that the cutting area is constant during a single revolution which facilitates its 2D description, however, they adopted another approach. They interpreted that the defect in the previous models is related to their incapability to simulate loads on cutters when bed boundaries are not normal to bit axis, the formation is nonhomogeneous, or the bit is whirling. They presented the formation as multiple radial layers, and each bit revolution removes a layer then all the forces are updated. This allowed them to assign different properties for the layer such as being tilted. They also allowed the bit to rotate around different points to accommodate for the bit's whirl. Their lab experiments showed that when the bit is penetrating another formation that has a tilted boundary, the variation in applied force on a bit cutter fluctuates massively before the bit is completely immersed in the new formation and the force stabilize. The same results were shown when they introduced some nodules in a sample to be drilled. Their model could also capture the variation in forces on cutters when the bit whirl and showed very high forces contribution as presented in **Figure 5** (Behr et al. 1993).

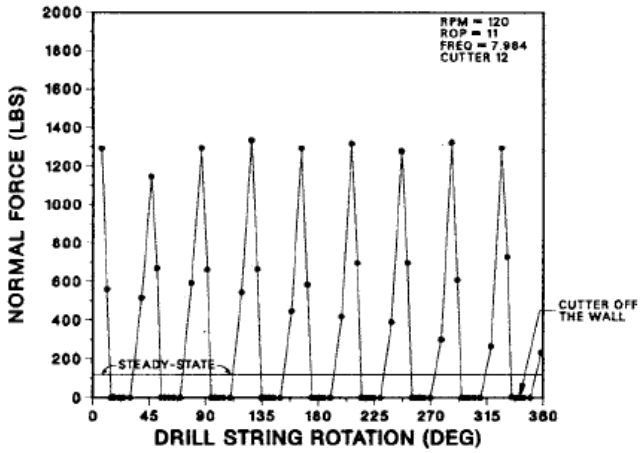

Figure 5: Behr et al. force capturing while bit is whirling (Behr et al. 1993)

Hanson and Hansen in 1995, modified Behr et al. model describing the formations penetrated by the PDC bit as vertically meshed grids. This allowed simulating more scenarios such as elevated rates of penetration (Hanson and Hansen 1995). In 2007, Endres improved the rock mesh representation compared to the previously mentioned models by considering a 3D triangulated surface where the vertices are updated after each bit revolution revealing a new position. This position update is function in the bit geometry (Endres 2007). In 2008, Chen, Collins and Thomas studied the bit walk mechanisms of the PDC bits. They used a 3D computer model to include all the factors that affect the bit walk. They applied a spherical coordinate to describe their model and succeeded to include the bit cutters effect in the model (Chen et al. 2008).

In 2011, Akbari et al. utilized the advances in finite element modelling to understand how the ROP of PDC bit cutter varies as a function in WOB and rotary speed. They studied the effect of oscillating WOB and found that ROP improvement was reduced as bottom hole pressure increased (Akbari et al. 2011). Hanson and Hensen model was also improved by Spencer et al. in 2013 to accommodate better drilling bits representation by introducing distributed contact modelling (Spencer et al. 2013).

Pryhorovska et al. constructed a finite element model using Ansys Explicit for the PDC bit cutter to study different kinds of cutter shapes and determine the shape with the least force imbalance as displayed in **Figure 6**. Their model showed that there was no difference between circular and linear cutting. They studied five different shapes of cutters and concluded that (Pryhorovska et al. 2015):

1. For all shapes, the force was randomly oscillating with no definite periodic pattern.
2. Oscillation amplitude increased with increasing the cutting depth, however, it did not follow a specific relationship.

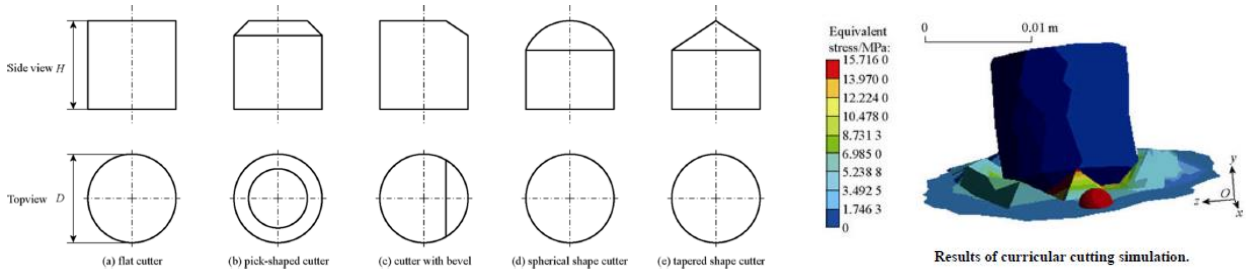

Figure 6: Pryhorovska et al. study (Pryhorovska et al. 2015)

Yari et al. also deployed the finite element method technique by utilizing ABAQUS CAE to study rock-PDC cutters interactions. They conducted two kinds of experiments, one with fixed depth of cut and the other was more realistic where the depth of cutter is

unfixed. The difference between both cases is shown in **Figure 7**. They proposed a new parameter to evaluate the drilling efficiency which represents the ratio between the cutting volume rate and the work done (Yari et al. 2018).

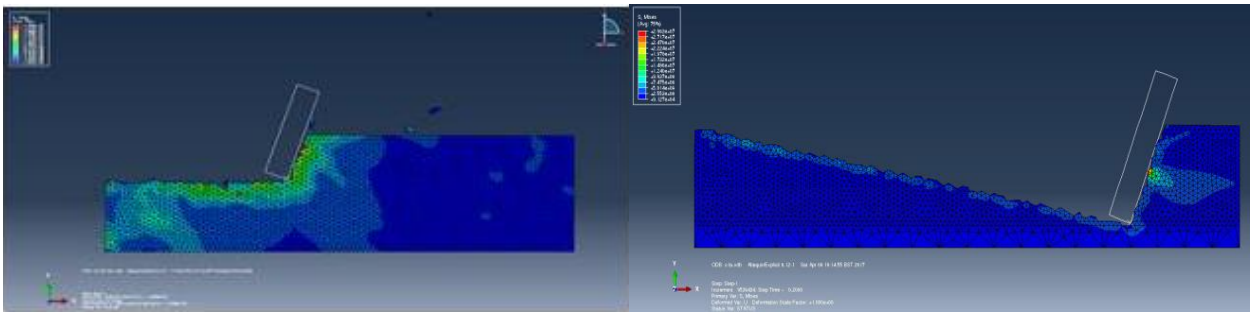

Figure 7: Yari et al. model for fixed and unfixed depth of cut (Yari et al. 2018)

Pelfrene et al. simulated the bit interaction with the hole being drilled as if it is a 3D mesh surface. They mentioned that when the bit motion affects the drill string motion, it should be simulated separately. Two classes of bit simulators were developed: 2D and 3D. 2D simulators are used to predict the PDC cutting sections assuming that the cutting section of each cutter is constant along a whole revolution which means that during a single revolution the ROP and RPM are unchangeable. Their drawback is that they cannot be used for roller cone bits or PDC bits with complex motion. Therefore, 3D bit simulators are used to overcome that. They introduced a new method to simulate any PDC bit geometry and formation in 3D including the cutting and not cutting parts of the bit. For PDC bits, the rock fails by elasto-plastic process, thereby, the volume of rock removed by the cutter can be approximated and the only parameter to determine is the interaction force. They determined the volume of rock removed by the aid of swept volume algorithm generating active surfaces that when connected give the trajectory of the cutter as can be presented graphically in **Figure 8**. They finally used their approach to improve bit design and future recommendations after making sure it matched with real data (Pelfrene et al. 2019).

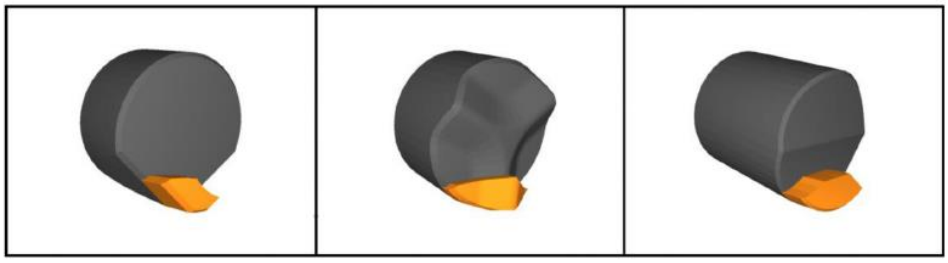

Figure 8: Pelfrene et al. generic swept volume algorithm (Pelfrene et al. 2019)

Huang et al. constructed a 3D full bit model to study the PDC bit-rock interaction aiming to improve the drilling of geothermal sources that are characterized by high stress, abrasiveness, and hardness. Their focus was simulating the impact drilling with a PDC bit. They as well depended on finite element method to build their model using ABAQUS (Huang et al. 2023).

Lumped-physics models

Before digging deeper into those mathematical formulations that attempt to resolve the PDC bit rock interactions numerically, some solid foundations must be introduced. All the intended to be illustrated models are based on forces resolving in the axial and tangential (longitudinal) direction with respect to the bit face. They all share the following assumptions, however, if a model deviated from those assumptions, it will be specifically mentioned for that model:

1. Shearing is the only rock failure mechanism
2. Rock is considered homogeneous, isotropic, with boundaries parallel to bit face perpendicular to the drillstring
3. The hole cleaning conditions are considered perfect with no redrilling of any rock fragments
4. The whole cutter surface area is engaged in the drilling process where the cutter surface area is equal to the cutting area
5. The cutter worn area is uniform and presented by a flat surface area
6. The friction force is only considered when the cutter is worn

In 1985, Ziaja introduced one of the first mathematical models of a PDC bit by considering bit wear as a function of forces resolved in two directions as presented in **Figure 9:** Ziaja's model (Ziaja 1985). He deduced the following equations that later used to conclude the WOB and torque on bit TOB.

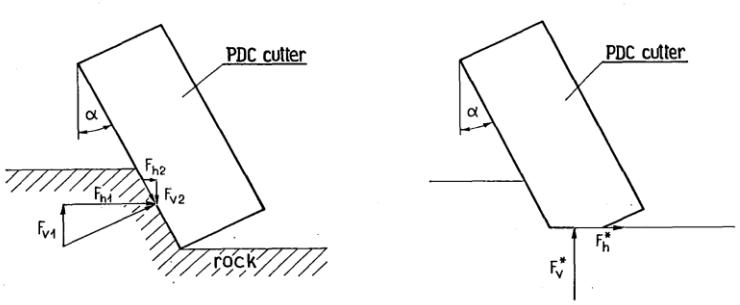

Figure 9: Ziaja's model

For new cutter,

$$F_{vc} = R_c S_c sin\alpha - \mu R_c S_c cos\alpha \tag{2}$$

$$F_{hc} = R_c S_c cos\alpha + \mu R_c S_c sin\alpha \tag{3}$$

For worn cutter,

$$F_{vc} = R_c S_c sin\alpha + R_P S_w \tag{4}$$

$$F_{hc} = R_c S_c cos\alpha + \mu^* R_P S_w \tag{5}$$

Where, F_{vc} and F_{hc} are the vertical and horizontal forces respectively, R_c is the rock resistance, R_p is the contact pressure, S_c is the cutting surface area approximated by cutter area, α is the rake angle and μ and μ* are the frictional factors in case of new and worn cutter respectively. He succeeded to estimate the WOB and TOB as well (Ziaja 1985).

In 1989, Warren and Sinor modelled the forces required by a single PDC cutter to remove a fixed rock volume then the integration for single cutter model to a bit model would result in the required WOB and TOB for a specific rate of penetration (ROP) (Warren and Sinor 1986). The model mainly depended on geometrical relationships to determine the cutter location. It could determine the WOB, TOB, and the volume removed by inputting the ROP, formation properties, and rotational speed. The model also considered cutter wear as seen in the following equations set (Warren and Sinor 1986).

$$F_N = \frac{\cos(\alpha - BR)}{1 - \sin(\alpha - BR)} \times d_w \times B_F \times RS \times d_{ce} \times C_1 + A_w \times RS \times C_2 \tag{6}$$

$$F_V = F_N \times \cos(\beta) \tag{7}$$

Where, A_w is average cutter wear rate, B_F is bit factor, BR is cutter back rake angle, C_1 & C_2 are constants, d_w is width of cut, d_{ce} is effective depth of cut, F_N is normal cutter force, F_V is normal components of cutting force, RS is the relative rock strength, α is angle of rock internal friction, and β is angle between bit axis and normal force (Warren and Sinor 1986).

In the case of worn cutters,

$$F_X = \frac{\sin(\alpha - BR)}{1 - \sin(\alpha - BR)} \times C_3 \times RS \times d_w \times d_{cm} + C_4 \times F_N \tag{8}$$

Where, C_3 & C_4 are constants, d_{cm} is mean depth of cut, F_X is cutting force in case of friction, and the first term after the equality represents a non-productive force waste on friction (Warren and Sinor 1986).

Detournay and Defourny studied the effect of WOB, TOB and angular velocity on ROP for the PDC bits (Detournay and Defourny 1992). In their model, the bit rock interaction is composed of two components which are the rock cutting and frictional component made by the friction beneath the cutter with the rock. The components of the force Fc are displayed in **Figure 10** for a sharp cutter and their expressions are presented in the next two equations, where A is cutting cross sectional area, ε is the rock specific energy and ζ is the vertical to horizontal force acting on the cutting face (Detournay and Defourny 1992).

$$F_s^c = \varepsilon A \tag{9}$$

$$F_n^c = \zeta\, \varepsilon\, A \tag{10}$$

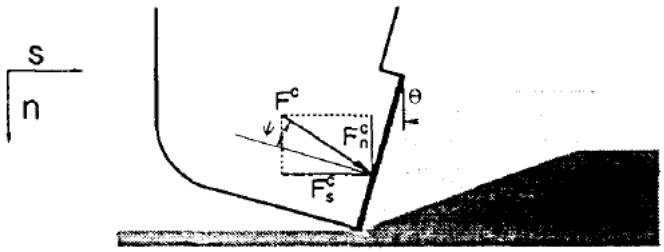

Figure 10: Detournay and Defourny model for a sharp cutter

For a worn cutter, the total cutter force F is decomposed into two vectorial components: F^c transmitted by the cutting face and F^f acting across the wear flat. For F^c the previous equations apply and for F^f the vertical F_n^f and horizontal F_s^f components are related by the coefficient of friction μ as seen in the following equation and schematic representation is **Figure 11** (Detournay and Defourny 1992).

$$F_s^f = \mu\, F_n^f \tag{11}$$

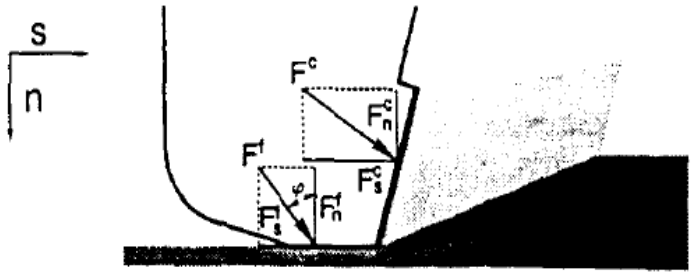

Figure 11: Detournay and Defourny model for a worn cutter

The more important component is F_s as it represents the force wasted in friction; therefore, the following relationship is derived,

$$F_s = F_s^c + F_s^f = \varepsilon\, A + \mu\, F_n^f \tag{12}$$

And,

$$F_n = F_n^c + F_n^f \rightarrow F_n^f = F_n - F_n^c \tag{13}$$

Therefore,

$$F_s = \varepsilon\, A + \mu\, (F_n - F_n^c) = \varepsilon\, A(1 - \mu\zeta) + \mu F_n \tag{14}$$

They define the specific energy E and drilling strength S by the following relations respectively,

$$E = \frac{F_s}{A}\ \&\ S = \frac{F_n}{A} \tag{15\&16}$$

For sharp cutter
$E = \varepsilon\ \&\ S = \zeta\, \varepsilon$

For worn cutter
$E = \varepsilon\,(1 - \mu\zeta) + \mu S \rightarrow E = E_O + \mu S$ (17&18)

They use the same data set Glowka and acquire better match for the measurements points according for their introduced relationships (Detournay and Defourny 1992).

They differentiate between E and ε, where the former is the specific energy for rock volume cut and the latter only represents the contribution of the cutting action to the specific energy. Thereby, they can calculate the efficiency by the ratio between both values as

presented in the following equation. The efficiency ranges from 0 when the cutter is just sliding on the rock surface to 1 for a perfectly sharp cutter (Detournay and Defourny 1992).

$$\eta = \varepsilon/E = F_s^c/(F_s^c + F_s^f) \tag{19}$$

They finally integrate the single cutter model into a generalized PDC bit model depending on splitting the WOB and TOB into two components following the force splitting theory in which component spent on cutting and another on friction.

$$T^c = \frac{1}{2}\varepsilon d a^2 \;\&\; W^c = \zeta \varepsilon \mathrm{da} \tag{20\&21}$$

Where, a is the bit radius and d is the depth of cut per revolution in which it is function in the rate of penetration *v* and the angular bit speed Ω and calculated by the next displayed equation (Detournay and Defourny 1992).

$$d = \frac{2\pi v}{W} \tag{22}$$

They defined a bit constant γ that describes the bit mechanical response according to its design and finally concluded the following bit model.

$$E = \varepsilon\,(1 - \beta) + \mu\gamma S \rightarrow E = E_O + \mu\gamma \mathrm{S} \tag{23}$$

Where, β is a parameter characterizing drilling process and equals to $\mu\gamma\zeta$ (Detournay and Defourny 1992).

Wojtanowicz and Kuru base their work on the assumptions that the bit is fully engaged with the whole down area and all cuttings are perfectly removed (Wojtanowicz and Kuru 1993). They neglect the impact of cutter wear on bit performance and assume that the formation boundary is normal to the bit face. They also study many cutter shapes and used empirical constants to account for this change and adjusting their original equations. They voluntarily ignore the effect of friction forces on the cutter side while deriving their model and present the equations below that represent the forces resolving in different directions as displayed in **Figure 12** (Wojtanowicz and Kuru 1993).

$$F_n = F_c sin\alpha + F_{fc} cos\alpha - F_w cos\alpha_c + F_{fw} sin\alpha_c \tag{24}$$

$$F_t = F_c cos\alpha - F_{fc} sin\alpha + F_{fw} cos\alpha_c - F_w sin\alpha_c \tag{25}$$

$$F_c = R_c A_c \tag{26}$$

$$F_c = \mu F_c = \mu R_c A_c \tag{27}$$

$$F_w = R_p A_w F_{fw} = \mu R_p A_w \tag{28}$$

$$F_h = F_t (cos\beta)^{-1} \tag{29}$$

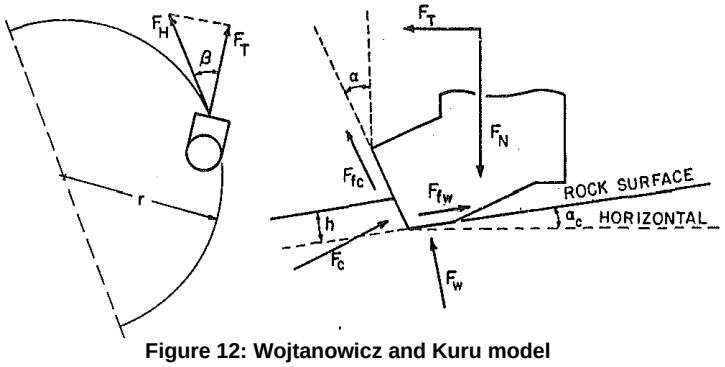

Figure 12: Wojtanowicz and Kuru model

Where, α is the back rake angle, α_c is the cutting angle, β is the side rake angle, μ is the coefficient of friction between cutter surface and rock, A_f is the abrasiveness constant, A_w is the cutter wear flat area, F_c is the cutting force, F_{fc} is the friction force acting on cutting surface area, F_{fw} is the friction force effective on wear flat area, F_h is the horizontal force at cutter, F_n is the normal force at cutter, F_t is the tangential force, F_w is the component of normal force acting on the wear flat area, R_c is the rock resistance to shearing, and R_p is the rock resistance to pressing (Wojtanowicz and Kuru 1993).

They derive two equations representing the ROP and TOB respectively as seen in the following equations. The model does not match fully field and laboratory data. The authors attribute this limitation to the assumption that cutter wear is neglected (Wojtanowicz and Kuru 1993).

$$R = k_3 h N^{a1} I \tag{30}$$

$$T^b = W E_1 \frac{1-\mu tg\alpha}{d_b(\mu+tg\alpha)} - A_w R_p E_2 \frac{2-(\mu+tg\alpha)^2}{\mu+tg\alpha} \tag{31}$$

Where, a1 is the rotary speed exponent, d_b is the bit diameter, E1 and E2 are constants calculated by integration, I is the cutters interference constant, N is the rotary speed, R is the drilling rate, h is cutting depth, k3 is the proportionality constant between penetration rate per one rotation and cutting depth, W is the weight on bit (Wojtanowicz and Kuru 1993).

Gerbaud et al. in 2006, introduced a model considering the cutter shape and size as well as whether it has chamfer or not and the forces resulted rock deformation due to the pressing of the cutter into the rock. In their model, they divided the forces into three groups as illustrated schematically in **Figure 13** where forces acting on the cutting face surface denote F^c, forces acting on the chamfer surface denote F^{ch} and forces acting on the back cutter surface denote F^b (Gerbaud et al. 2006).

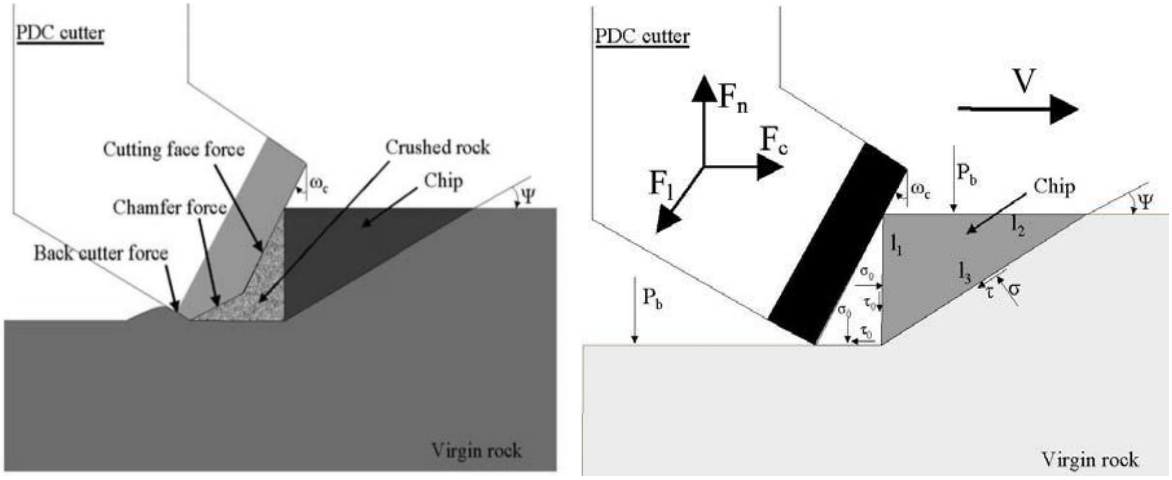

Figure 13: Gerbaud et al. model

F^c is the component which fails the rock. The chamfer is applied to PDC bits to increase its fracture resistance when drilling harder formations by reducing the stress concentration at the tip of the cutter, the F^{ch} is function in the cut height. The F^b is the same as the friction force addressed previously in literature. Based on these considerations, they introduced a set of equations describing the components for each force denoting them as the cutting force F_c and normal force F_n (Gerbaud et al. 2006).

For cutter face force,

$$F_c^c = R_{eq} A \tag{32}$$

$$F_n^c = \tan(\theta + \omega_c) R_{eq} A \tag{33}$$

For chamfer force,

$$F_c^{ch} = \sigma_0 \tan(\varphi') A_{ch} \tag{34}$$

$$F_n^{ch} = \sigma_0 A_{ch} \tag{35}$$

For back cutter face (friction force), empirical correlations were deployed where,

$$F_c^b = \sigma_0 \, f(\alpha, d, \omega_d) \tag{36}$$

$$F_n^b = F_c^b \, f_1(\alpha, d, \omega_d) \tag{37}$$

Where, α is the repression angle, θ_f is the rock-cutter friction angle, σ_0 is the hydrostatic stress into the crushed zone, ω_c is the back rake angle, ω_d is the relief angle, A is the cross section area of the cut, A_{ch} is the chamfer surface area on a horizontal plane, d is the depth of cut, F^b is the force acting upon the back cutter face, F^c is the force acting upon the cutter face, F_c is the PDC cutting force, F^{ch} is the force acting upon the cutter chamfer, F_f is the force acting upon the PDC wear flat and R_{eq} is the rock intrinsic specific energy (Gerbaud et al. 2006).

In 2008, Detournay et al. completed the previous work they published in 1992 with the goal of predicting the resultant forces on a bit and started by categorizing the PDC bit cutting process into 3 phases (Detournay et al. 2008):

- Phase 1: friction force is dominant, and it occurs when the cutter has low depth into the formation
- Phase 2: it occurs when the contact forces are fully mobilized
- Phase 3: it occurs when the contact between the formation and cutter increases due to insufficient hole cleaning

They defined two new quantities that are l, the contact length that represents the measure of the wear flat length and σ, which is the contact strength which is maximum normal stress that can be transmitted to the cutter, to better describe the friction process (Detournay et al. 2008). Their previous work did not mention explicitly a full set of equations predicting the torque and rate of penetration to the applied weight on bit and angular velocity and was left for the user to derive (Detournay and Defourny 1992), which they overcome in the newer study (Detournay et al. 2008).

They agreed that the dynamic quantities of WOB and TOB are w and t respectively and defined them as seen in the following equations and graphically on **Figure 14** (Detournay et al. 2008).

$$w = \frac{WOB}{a\,(1-\rho)} \;\&\; t = \frac{2T}{a^2(1-\rho^2)} \tag{38\&39}$$

Where, a is the bit diameter and ρ is the ratio between the inner to the outer bit radius. By including those variables, they accounted for the bit dimensions in their model (Detournay et al. 2008).

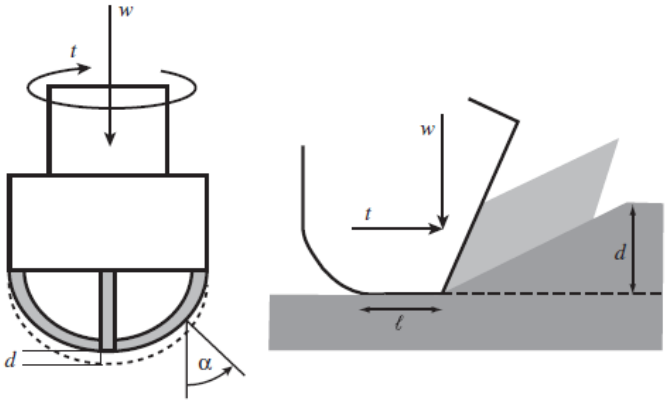

Figure 14: Detournay et al. model

Following the previously demonstrated equations,

$$t = t_c + t_f \;\&\; w = w_c + w_f \tag{40\&41}$$

$$t_c = \varepsilon d \;\&\; w_c = \zeta \varepsilon d \tag{42\&43}$$

They defined the vertical to horizontal force acting on the cutting face ζ by,

$$\zeta = \tan(\psi + \theta) \tag{44}$$

where, ψ is the friction angle and θ is the back rake angle and they are both dependent on each other. When it ζ and $\mu\gamma$ are known, all the components of t and w can be calculated. All parameters graphical representation is shown in **Figure 15** (Detournay et al. 2008).

$$t_c = \frac{t-\mu\gamma w}{1-\beta} \,\&\, t_f = \mu\gamma w_f \tag{45\&46}$$

$$w_c = \zeta t_c \,\&\, w_f = \frac{w-\zeta t}{1-\beta} \tag{47\&48}$$

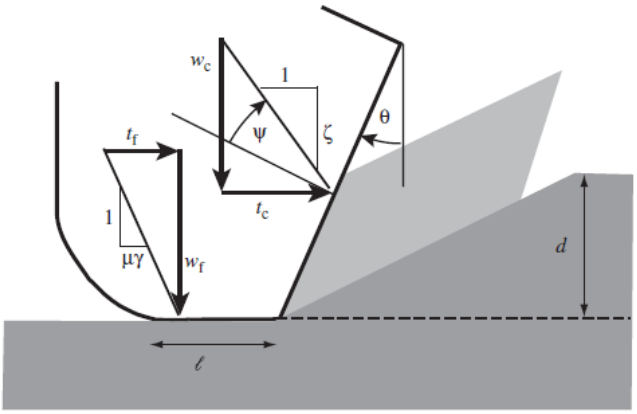

Figure 15: Detournay et al. model

They provided mathematical model supported by geometrical illustration for phase 1 and 2 as presented below (Detournay et al. 2008).

Phase 1 – The response equations for this phase are derived on the assumption that the contact component of the weight, w_f, increases linearly with the depth of cut, d.

$$w_f = \sigma k d \tag{49}$$

And,

$$w = w_f + w_c \tag{50}$$

Therefore,

$$w = \sigma k d + \zeta \varepsilon d = d\, S \star \tag{51}$$

$$t_f = \mu\gamma\sigma k d \tag{52}$$

And,

$$t = t_f + t_c \tag{53}$$

Therefore,

$$t = \mu\gamma\sigma k d + \varepsilon d = d\, E \star \tag{54}$$

Where, k represents the rate of change of contact length with the depth of cut.

Phase 2 – The governing equation was found to be as follows (Detournay et al. 2008).

$$w = \zeta t + (1-\beta)\sigma\ell \tag{55}$$

Phase 3 – The contact area between the bit and the rock increases due to the accumulation of sheared rock material caused by poor cleaning. The transition to this phase occurs at a critical depth of cut which is function in bit geometry, mud flow rate, and properties of the rock being drilled with no numerical model describing that explicitly (Detournay et al. 2008).

Che et al. adopt the theory that PDC bits fail rocks not only because of shearing but crushing as well. They devised their model considering the powdery chips formed beneath the cutter and named it Tip Crushing Zone (TCZ) where a fracture is initiated and propagates in arbitrary direction. They believe that the failure of rock in the TCZ that forms the powder chips is equal to the rock uniaxial compressive strength (σ_c) and the formation of the large normal chips formed by the shearing is equal to the formation tensile strength (σ_t). They neglect the effect of friction and cutter speed. Their considerations can be schematically presented in **Figure 16** displayed below (Che et al. 2016).

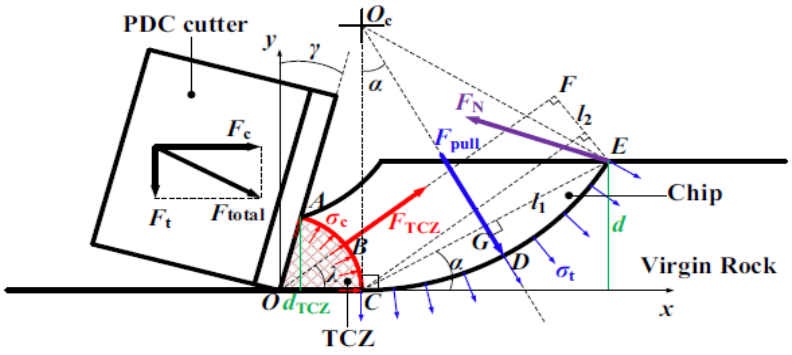

Figure 16: Che et al. model

They define the force acting on the TCZ (F_{TCZ}) by the following formula,

$$F_{TCZ} = 2w\sigma_c \frac{d_{TCZ}}{cos\gamma} \sin\left(\frac{\pi}{2} - \frac{\gamma}{2}\right) \tag{56}$$

Where, γ is the back rake angle, d_{TCZ} is depth of TCZ, and w is the cutter width.

And the force responsible for the chipping (F_{pull}) by,

$$F_{pull} = \frac{\sigma_t d}{sin\alpha} \tag{57}$$

Where, α is the crack initiation angle, and d is depth of cut.

And the total cutting force Fc can be calculated by,

$$F_c = w\sigma_c d \cos\gamma \left[\frac{-cos\gamma}{4sin^2\left(\frac{\pi}{4}-\frac{\gamma}{2}\right)+4\frac{\sigma_t}{\sigma_c}} - \frac{\sqrt{cos^2\gamma+4\frac{\sigma_t}{\sigma_c}sin^2\left(\frac{\pi}{4}-\frac{\gamma}{2}\right)+4sin^4\left(\frac{\pi}{4}-\frac{\gamma}{2}\right)}}{4sin^2\left(\frac{\pi}{4}-\frac{\gamma}{2}\right)+4\frac{\sigma_t}{\sigma_c}} + \frac{\sqrt{\frac{\sigma_t}{\sigma_c}+1}}{2sin\left(\frac{\pi}{4}-\frac{\gamma}{2}\right)} + \frac{1}{2}\cot\left(\frac{\pi}{4}-\frac{\gamma}{2}\right) \right] \tag{58}$$

They finally argue that the cutting force is not linearly proportional to the depth of cut except for shallow cuts only (Che et al. 2016).

Huang et al. study the ROP for PDC bits before and after cutters wearing depending on numerical simulation. The aim of their study is to utilize the numerical simulation to predict the cutters wearing performance and within their research they modelled the force system for the PDC bit-rock interaction as shown in the following equations (Huang et al. 2017).

$$F_t = e^{\frac{H_d}{d\,cos\alpha}} p_t K^{q_t} A^{0.7564} \frac{l}{l_d} \tag{59}$$

$$F_a = e^{\frac{H_d}{d\,cos\alpha}} p_a K^{q_a} A^{0.5472} \frac{l}{l_d} \tag{60}$$

$$p_t = 0.481e^{6.9291\,sin\alpha};\ q_t = 2.4154(cos\alpha)^{4.8154} \tag{61}$$

$$p_a = 4.832e^{3.1724\,sin\alpha};\ q_a = 1.8196(cos\alpha)^{1.6419} \tag{62}$$

Where, α is the back rake angle, A is the cutter surface area, d is the cutter diameter, K is the drillability factor, l is the real length of cutting arc, l_d is the equivalent length of cutting arc, and Hd is the worn height of cutter (Huang et al. 2017).

Atashnezhad et al. claim that neglecting the interfacial angle , which is the angle representing the frictional interaction between the cutter face and the rock during the cutting process, in ROP estimation results in errors; therefore, they design a single cutter model considering this parameter and use it as the base to develop a full PDC bit model. They calculate the volume of rock removed theoretically by computing the product of area ahead of the cutter, rotary speed, and effective radius. The new model is presented by the following equations (Atashnezhad et al. 2020).

$$ROP = C_b\, NOC \left(\frac{5\, RPM\, \pi\, R_e\, A_v}{A_B}\right) \tag{63}$$

$$A_v = \left(\left(\left(\frac{D_c}{2}\right)^2 \times \cos^{-1}\left(\frac{\frac{D_c}{2} - \frac{\left(\delta + \frac{BG\, D_c \cos(BR)}{8}\right)}{\cos(BR)}}{\frac{D_c}{2}}\right) - \left(\frac{D_c}{2} - \frac{\left(\delta + \frac{BG\, D_c \cos(BR)}{8}\right)}{\cos(BR)}\right) \times \sqrt{2 \times \frac{D_c}{2} \times \frac{\left(\delta + \frac{BG\, D_c \cos(BR)}{8}\right)}{\cos(BR)} - \left(\frac{\left(\delta + \frac{BG\, D_c \cos(BR)}{8}\right)}{\cos(BR)}\right)^2}\right) - \left(\left(\frac{D_c}{2}\right)^2 \times \cos^{-1}\left(\frac{\frac{D_c}{2} - \left(\frac{BG\, D_c}{8}\right)}{\frac{D_c}{2}}\right)\right) - \left(\frac{D_c}{2} - \frac{BG\, D_c}{8}\right) \times \sqrt{2 \times \frac{D_c}{2} \times \frac{BG\, D_c}{8} - \left(\frac{BG\, D_c}{8}\right)^2}\right) \times \cos(BR + \psi_{Full\ bit}) \times \cos(SR) \tag{64}$$

Where, $\psi_{full\ bit}$ is the full bit interfacial friction angle, BR is the back rake angle, BG bit grade, δ is the cutter depth of cut, A_B is the bit face area, A_v is the cutter front area, D_c is the cutter diameter, NOB is the number of blades, and R_e is the equivalent radius (Atashnezhad et al. 2020).

Later in 2020, Li et al. developed a single cutter force model for PDC bits. Their model can predict the effect of the principal stresses and rock strength on the resultant force. Their model depends on Nishimatsu's model, as seen in the below equations, as their starting point then integrated the rock stresses. They support their findings with experiments that also show the effect of cutting angle and mud pressure on the cutting force (Li et al. 2020).

$$F = \frac{2}{n+1}\tau_m h \frac{cos\varphi_k}{\cos(\varphi+\theta+\varphi_k)+1} \tag{65}$$

$$F_\sigma = F \sin\left(\frac{1}{2}(\varphi + \theta - \varphi_k)\right) \tag{66}$$

$$F_\tau = F \cos\left(\frac{1}{2}(\varphi + \theta - \varphi_k)\right) \tag{67}$$

Where, F is the resultant force on the failure line, Fσ is the normal component of the resultant force F on the failure line AB displayed on Error! Reference source not found., Fτ is the tangential component of the resultant force F on the failure line AB, h is the depth of the cut, n is the coefficient related to the parameters of cutting teeth, θ is the cutting angle of the PDC cutter, φ is the angle between direction of resultant force PL at point A and the front edge of the PDC cutter, τm is the shear strength of rock, and φk is the friction angle of rock (Li et al. 2020).

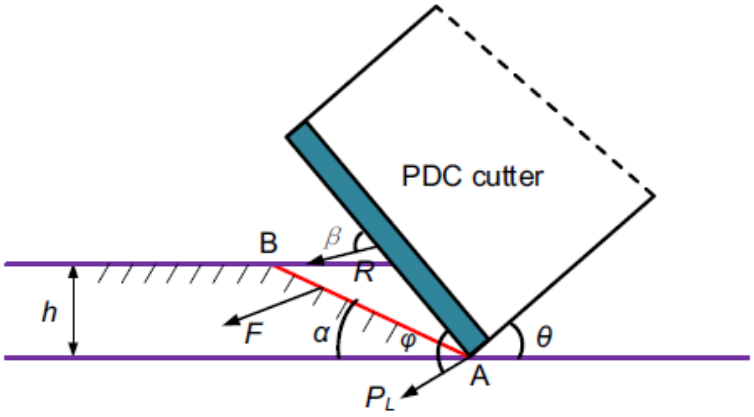

Figure 17: Li et al. model

Wei et al. in 2024, study single cutter-rock failure behavior and integrate that into a full bit model. They managed to define the cutter contact area responsible for rock failure. They model the brittle rock failure when the depth of cut exceeds a definite threshold length as seen in the following equations system illustrated by the **Figure 18** (Wei et al. 2024a, 2024b).

$$F_{resb} = F_{basic} + F_{chip} \tag{68}$$

$$F_{chip} = \frac{1}{L}(F_{chipmax} - F_{basic}) \tag{69}$$

$$F_{basic} = b\, r \cos^{-1}\left(\frac{r - D/\cos\alpha}{r}\right) \tag{70}$$

$$F_{chipmax} = c\left[r^2 \sin^{-1}\left(\frac{\sqrt{r^2-\left(r-\frac{D}{\cos\alpha}\right)^2}}{r}\right) - \left(r - \frac{D}{\cos\alpha}\right)\left(\sqrt{r^2 - \left(r - \frac{D}{\cos\alpha}\right)^2}\right)\right] \tag{71}$$

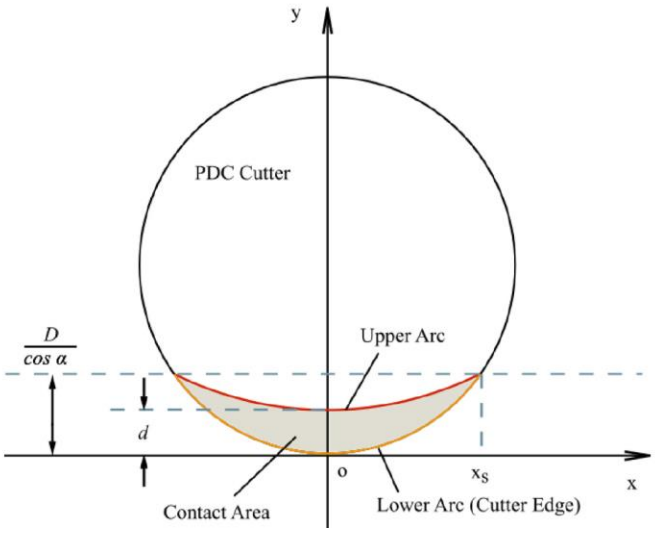

Figure 18: Wei et al. model

Where, α is the back rake angle, b and c are fitting coefficients, F_{resb} is the cutting force, F_{basic} is the basic cutting force, F_{chip} is the incremental cutting force as the PDC cutter advances, *L* is the total travel length of the cutter in one cutting period and r is the cutter diameter (Wei et al. 2024a, 2024b).

Python library for PDC bit models

Several of the models presented in the preceding section are included in the ***PyDrill*** library, an open-source drillstring dynamics library available via the Open Source Drilling Community (Shor et al. 2022). In this section, the implementation and verification of the full bit rock interaction models are detailed.

Ziaja's model(Ziaja 1985)

The model requires the following properties: required rock properties include Rc that is the index of rock strength for cutting and Rc that represents the index of rock strength for cutting. The bit properties include number of cutters (nc), diameter of PDC cutter (dc), depth of cut (h), linear wear of PDC cutter (x), rake angle (α), and side angle (β). Those properties ae used to calculate the cutting surface area of the cutter (Sc) and the worn surface area (Sw). The resultant WOB and TOB can then be calculated and finally to calculate the ROP and assumed RPM will be inputted to the model along with the nc and h. **Figure 19:** Ziaja's model approach presents a flow chart explaining the whole process applied.

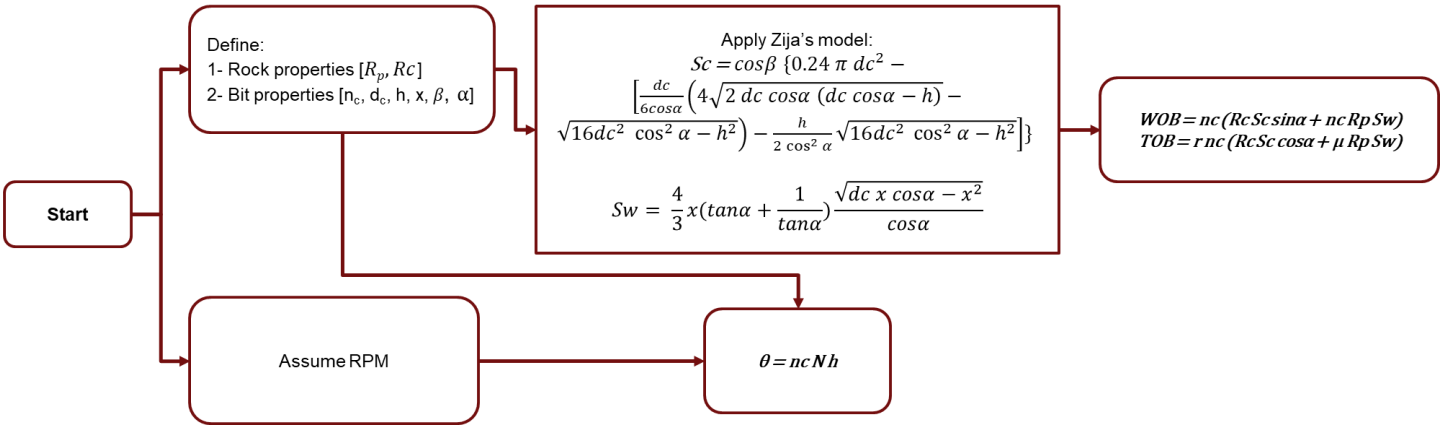

Figure 19: Ziaja's model approach

Detournay et al. model (Detournay and Defourny 1992, Detournay et al. 2008)

The full bit model designed by Detournay et al. is implemented in two ways:

The first approach is seen in **Figure 20:** Detournay et al. model, 1st approach. This approach follows a similar construction to Ziaja's, where the rock properties including specific energy (ε), friction factor (μ), and the ratio of vertical to horizontal forces (ζ) simultaneously with the bit properties including bit radius (a), bit constant (γ), the maximum normal stress that can be transmitted to the cutter (σ), and the contact length that represents the measure of the wear flat length (ℓ). The WOB and TOB measured from the surface and corrected to the bit position are also used as inputs. This data is used to determine the depth of cut from the WOB_c and TOB_c used in the cutting action. The two values of the calculated depth of cut are averaged. Assuming and RPM the average depth of cut is used to calculate the ROP.

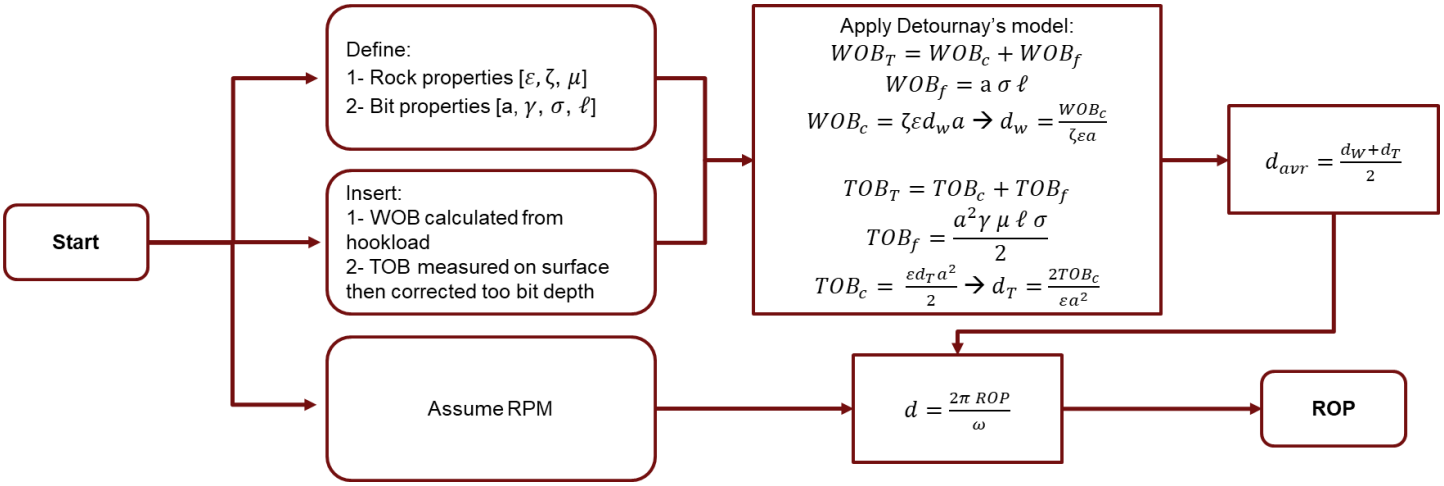

Figure 20: Detournay et al. model, 1st approach

The second approach is designed in a way that the required ROP will be treated as an input with the rock properties, bit properties and RPM assumption. These inputs are intended to be used to calculate the WOB and TOB that should be applied to acquire this ROP. **Figure 21:** Detournay et al. model, 2nd approach shows the methodology of attaining these results.

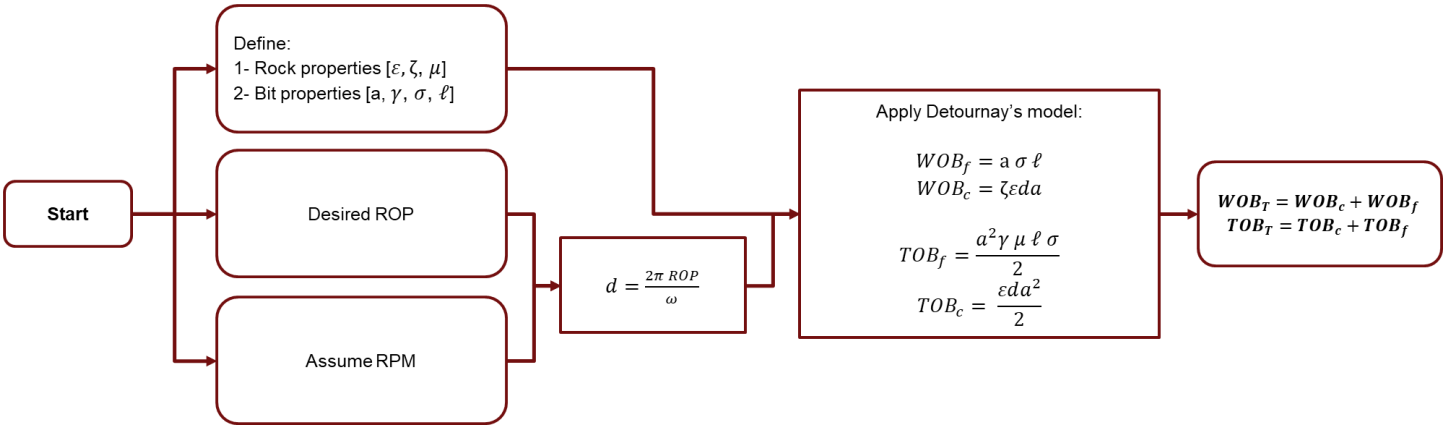

Figure 21: Detournay et al. model, 2nd approach

Wojtanowicz and Kuru model (Wojtanowicz and Kuru 1993)

As a significant number of parameters and experimentally determined coefficients is required, this model is not included in the open source library as these parameters will likely rarely all be known with a high degree of confidence.

Gerbaud et al. force model (Gerbaud et al. 2006)

This model considered the forces acting on the bit without attempting to formulate the ROP. To apply this model, aid from Ziaja's model and Detournay et al. model will be used as will be explained shortly. It is important to mentioned that the forces in this model are resolved into normal and tangential forces and each one of those has four components that are the cutting force, the chamfer force, the back cutter force, and friction force in case of cutters wear. Each force is computer for a single cutter. In this approach the back cutter force is neglected because it is determined experimentally in an empirical fashion. This means that the rock properties, including cut area (A), hydrostatic stress (σ_0), back rake angle (ωc), Rock-cutter friction angle (θ_f), along with bit properties, summarized by bit radius (a) and chamfer projected area (A_{ch}), are used to calculate the total cutting force. Ziaja's model only comes to action when the cutter is worn to calculate the wear area.

The cutting force is then used to be equated with WOB_c calculated from Detournay et al. model using the number of cutters (nc) as the scaling factor, resulting in the anticipation of the depth of cut. Given the depth of cut and an assumption of the RPM, Detournay et al. model is applied once more to deduce the ROP. **Figure 22:** Gerbaud et al. force model + Ziaja's model + Detournay et al. ROP model summarizes the steps taken to accomplish this approach.

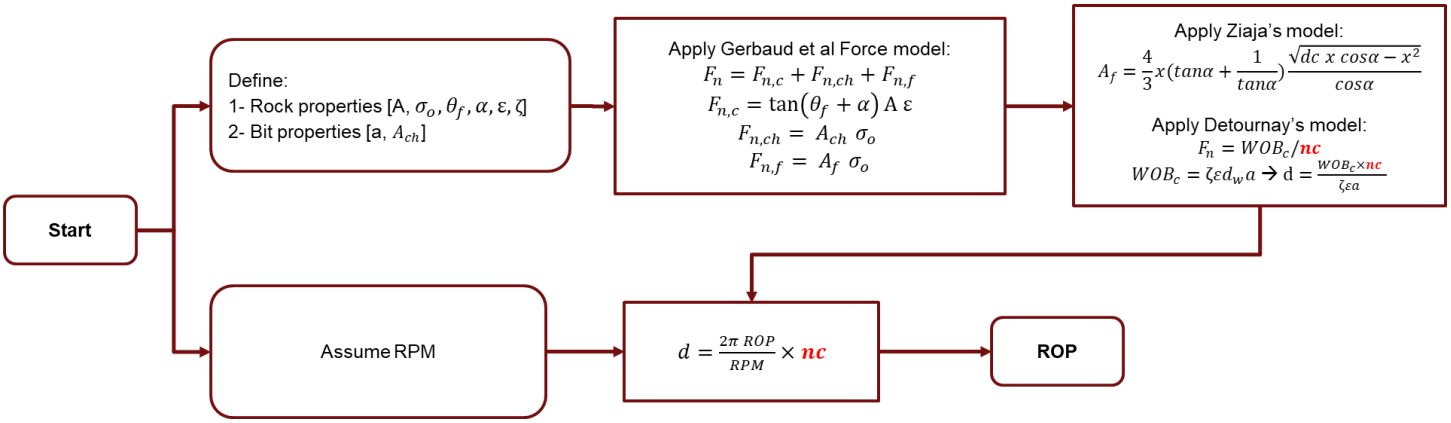

Figure 22: Gerbaud et al. force model + Ziaja's model + Detournay et al. ROP model

Che et al. force model (Che et al. 2016)

This model explicitly resolved the forces encountered during drilling by PDC cutter. However, it was not expanded to conclude the desired ROP as the previous model. Therefore, considering the methodology of forces formulation Che et al. adopted, Detournay et al. model will be then used reach the required ROP. This approach is better explained by considering **Figure 23:** Che et al. force model + Detournay et al. ROP model.

The vertical force used in cutting is computed as function in rock uniaxial compressive strength (σc), tensile strength (σt) and cutter width (w). The WOB, which represents the axial force measured from the hookload is then used as an input. Detournay et al. model is

used to define the WOB_c used in cutting. Equating the WOB_c and the cutting force allows the calculation of the depth of cut which with further application of Detournay et al. model, the ROP is detected same as carried out in anticipating the ROP from Gerbaud et al. force model.

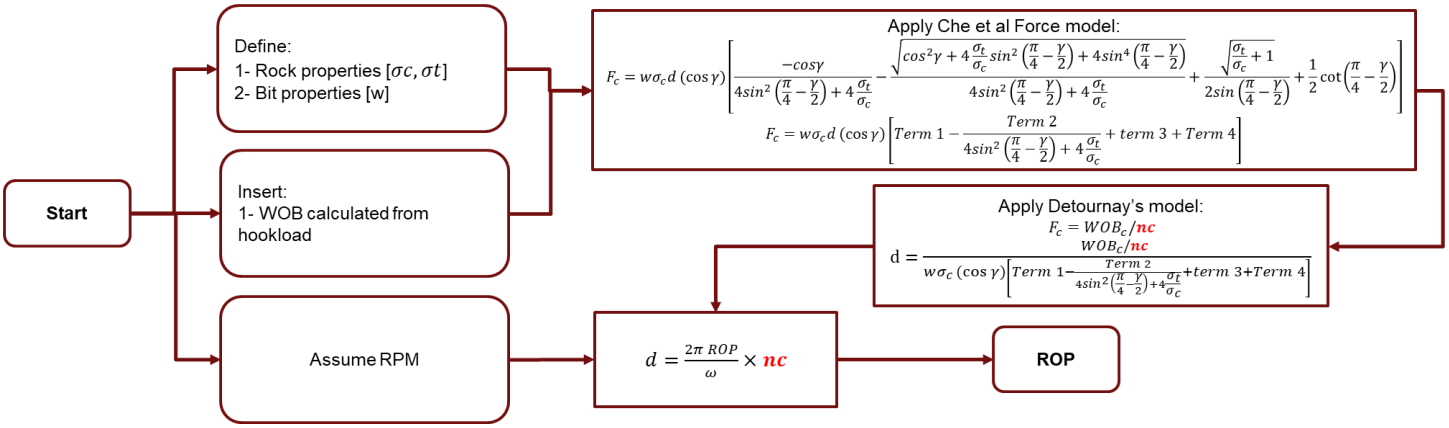

Figure 23: Che et al. force model + Detournay et al. ROP model

Results and discussion

The required bit and formation parameters and model outputs are summarized in Table 1: Summary table for inputs & Table 2: Summary table for outputs.

Table 1: Summary table for inputs

Input	Detournay	Ziaja	Che	Gerbaud
Rotational speed (rpm)	✓	✓	✓	✓
Bit radius (inches)	✓			✓
Cutter diameter (dc) (inches)		✓		✓
Back rake angle (alpha) (°)		✓	✓	✓
Side rake angle (beta) (°)		✓		
Rock-cutter friction angle (theta) (°)				✓
Radial location (r) (inches)		✓		
Number of cutters (nc)		✓		
Depth of cut (d) (inches)	✓	✓	✓	
Cutter width (w) (inches)			✓	
Length of wear flat (inches)	✓	✓		✓
Rate of Penetration (ROP) (ft/hr)	✓			
Rock intrinsic energy (lbf/in²)	✓			✓
Rock compressive strength (sigma_c)			✓	
Rock tensile strength (sigma_t)			✓	
Index of rock strength for cutting Rc (Ibf/in²)		✓		
Index of rock strength for pressing Rp (Ibf/in²)		✓		

Max contact pressure (lbf/in²)	✓		✓	
Total WOB (WOB_total) (lbf)	✓		✓	
Total TOB (TOB_total) (lbf.ft)	✓			
Chamfer area (A_ch) (inches²)				✓
Cutting area (A) (inches²)				✓
Hydrostatic stress into the crushed zone (sigma_0)				✓
Zeta (ζ) (unitless)	✓			✓
Mu (friction factor) (unitless)	✓			
Bit constant (unitless)	✓		✓	
Empirical constant (k)				✓

Table 2: Summary table for outputs

Output	Detournay	Ziaja	Che	Gerbaud
Total WOB (WOB_total) (lbf)	✓	✓		
Total TOB (TOB_total) (lbf.ft)	✓	✓		
Rate of Penetration (ROP) (ft/hr)	✓	✓	✓	✓

High density of parameters is required to be input for these four models application, hereby, the Utah Frontier Observatory for Research in Geothermal Energy **(**FORGE) public dataset published by the U.S. Department of Energy (DOE) (2023) is utilized to ensure that the code is running properly, where well 56-32 and 58-32 data were used. Some of the inputs are calculated as will be illustrated in the coming section.

The FORGE, managed by the University of Utah's Energy & Geoscience Institute and sponsored by the DOE, is a dedicated underground laboratory near Milford, Utah. It focuses on developing, testing, and accelerating breakthroughs in enhanced geothermal systems (EGS) technologies. The project aims to establish reproducible, commercial pathways for EGS, enabling the extraction of geothermal energy from hot, dry rock formations that are otherwise non-productive. By providing a controlled environment for innovative research and robust data collection, Utah FORGE plays a pivotal role in advancing geothermal energy as a sustainable and widely applicable resource (2023).

The input data file to the code contains all the parameters presented in Table 1. The in-hand data extracted from the mentioned dataset are as follows,

- Rotational speed (RPM)
- Bit radius (in)
- Rate of penetration (ft/hr)
- Weight on bit (Ibf)
- Cutter diameter (in)
- Number of cutters (Unitless)
- Friction factor (Unitless)
- Index of rock strength for cutting (psi)
- Index of rock strength for pressing (psi)
- Rock compressive strength (psi)
- Rock tensile strength (psi)
- Friction angle (deg)

Due to the incompleteness of data, some parameters are assumed, and others are calculated in which they are presented below as follows,

- Length of wear flat (in) – based on the bit run record, the bit used for drilling 2919 ft in single run starting at depth starting at depth 390 ft and ends at depth 3309 ft. When it was pulled out of hole, the damage was classified as coring with inside damage 8. Therefore, the wear is assumed to be linear across the whole section with total damage at 50% cutter wear.
- Ratio of vertical to horizontal forces assumed to be 1
- Back rake angle assumed to be 12 deg
- Side rake angle assumed to be 5 deg
- Rock intrinsic energy (psi) is calculated using the following formula,

$$\frac{WOB}{A} \tag{72}$$

- Torque on bit is calculated using the formula presented below,

$$\frac{\varepsilon\ ROP\ A}{RPM} \tag{73}$$

- Depth of cut is estimated using the formula below,

$$\frac{ROP}{RPM\ n_c} \tag{74}$$

- Ratio between the projection of the crushed zone on the surface and cutting area (k) assumed to be 1
- Hydrostatic stress (psi) is approximated by the hydrostatic pressure of mud and calculated by the following formula,

$$\sigma_o = 0.052\ \rho_m(8.8\ ppg)h \tag{75}$$

- The chamfer properties, mainly the area, were neglected as there was no data about the cutters' chamfer
- All the cutters considered are disc shaped, therefore the cutter width is equal to cutter diameter
- The cross-sectional area of the cut is approximated by depth of cut multiplied by the cutter width
- Bit constant is assumed to be 1

Error! Reference source not found. reflects the real data of the section drilled. The plots show the minimum, maximum and average values for each parameter. The average is calculated for every 100 ft.

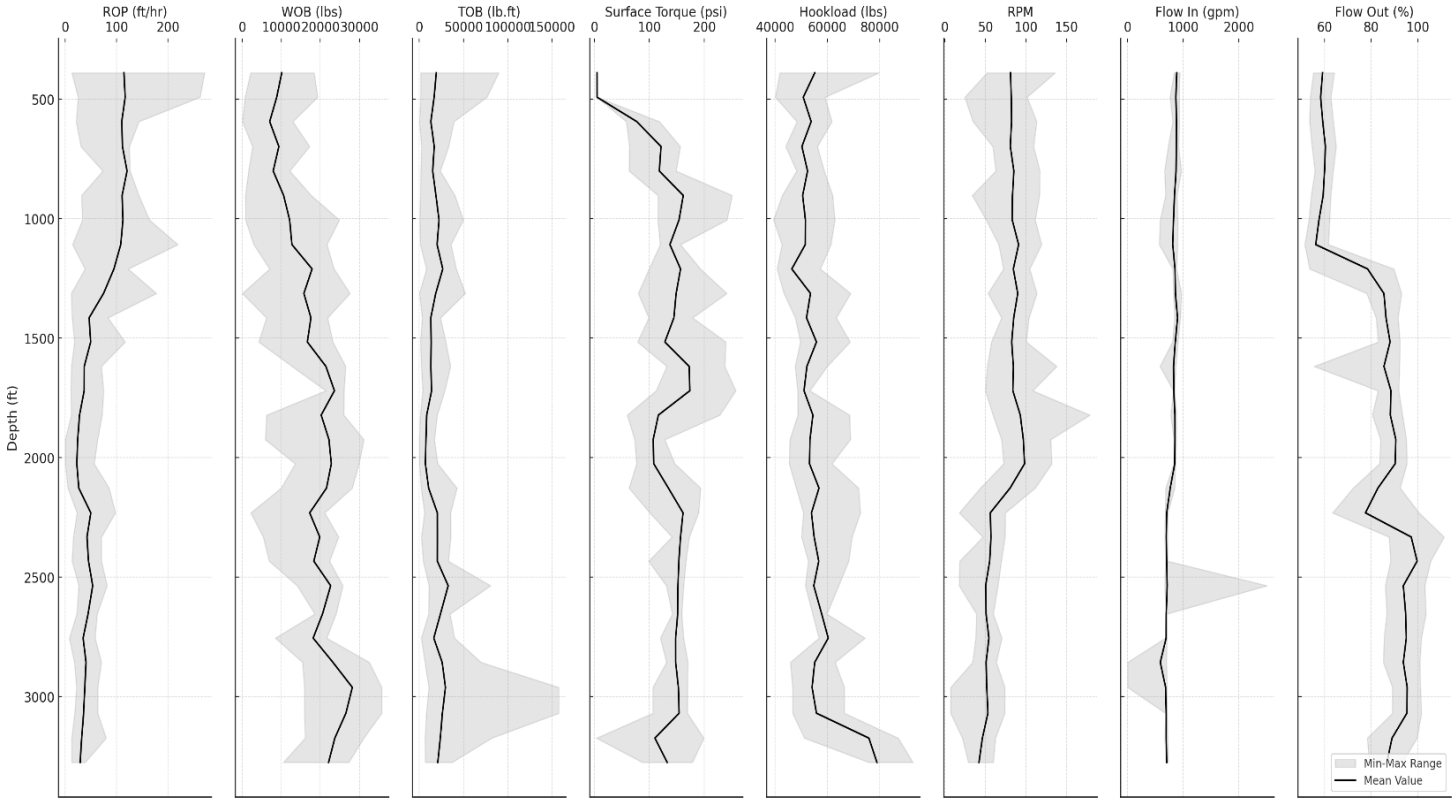

Figure 24: Real drilling data

Three sections of the total footage drilled are selected at the top, middle and bottom of section as seen in **Figure 25:** Section selection that represents the ROP real data, to examine the variation in models behavior with respect to the ROP variation that is relatively decreased due to cutters wearing.

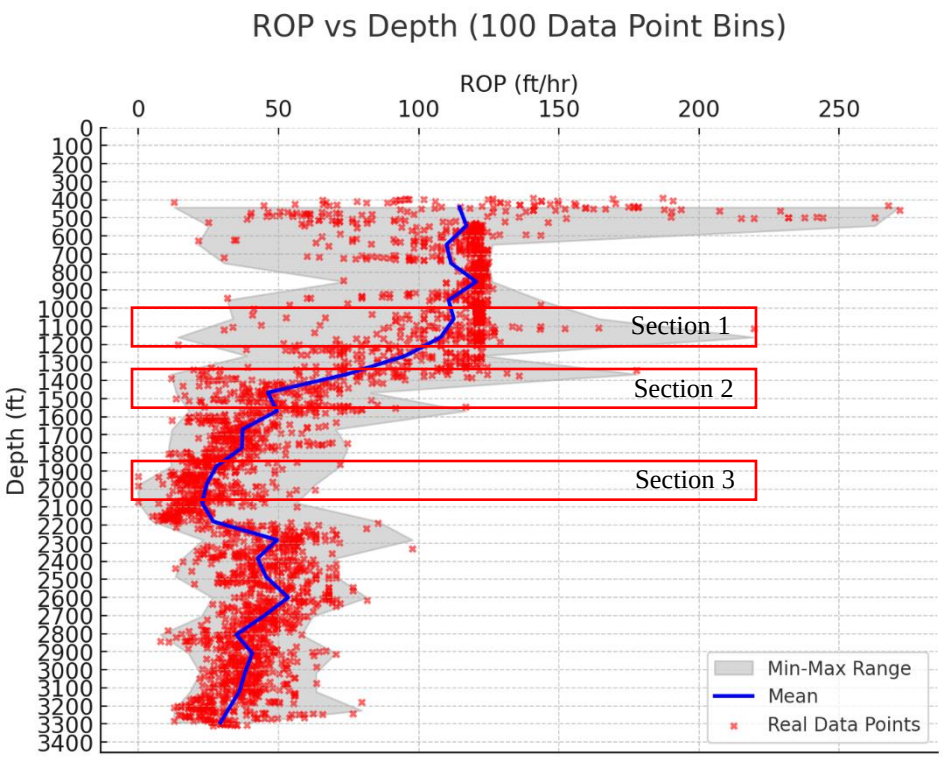

Figure 25: Section selection

The output ROP from the code calculated from different models are plotted against the real ROP for the 3 sections, each model at a time. **Figure 26:** Real vs Detournay et al. ROP model comparison represents the ROP from Detournay et al. model, where it shows a good agreement in sections one and two where the wear is still small compared to the higher wear expected at section three. This can also be concluded by comparing the average values trend.

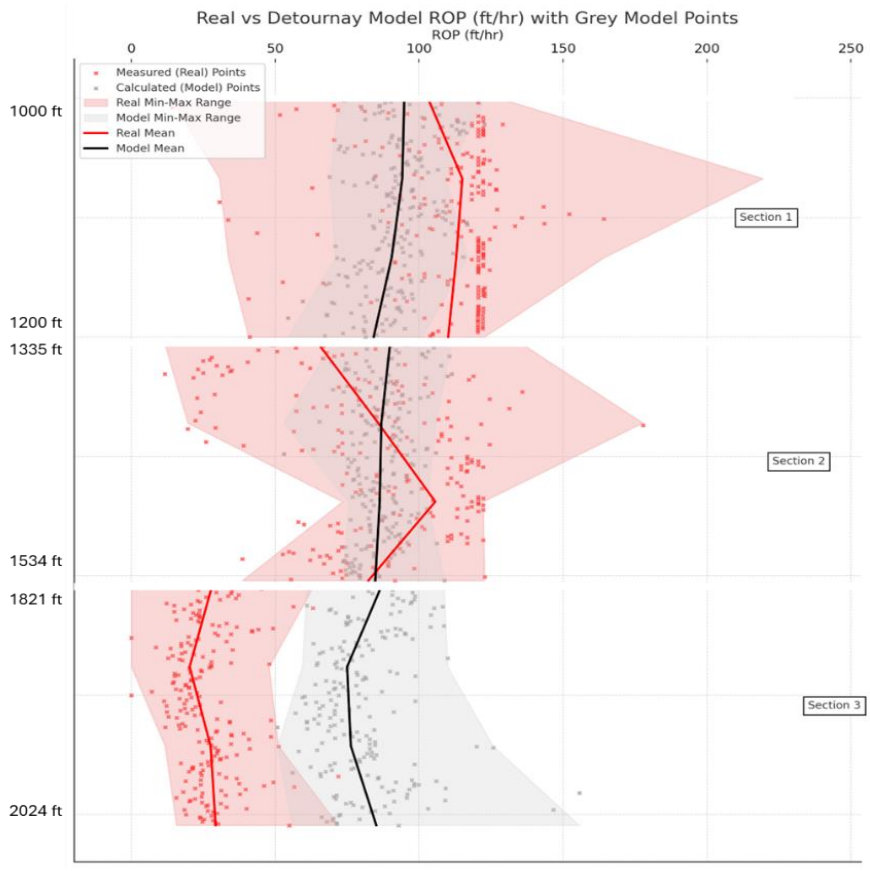

Figure 26: Real vs Detournay et al. ROP model comparison

Gerbaud's ROP model shown in **Figure 27:** Real vs Gerbaud ROP model comparison shows over estimation of the ROP along the three sections. This is somehow expected due to the assumption made earlier, where the back cutter force is not integrated into the code as it is determined experimentally, and such data is not available. This force is not spent on cutting action which means that it will reduce the ROP when incorporated. Also, the chamfer effect is neglected where the chamfer area is assumed to be zero in the code due to lack of data.

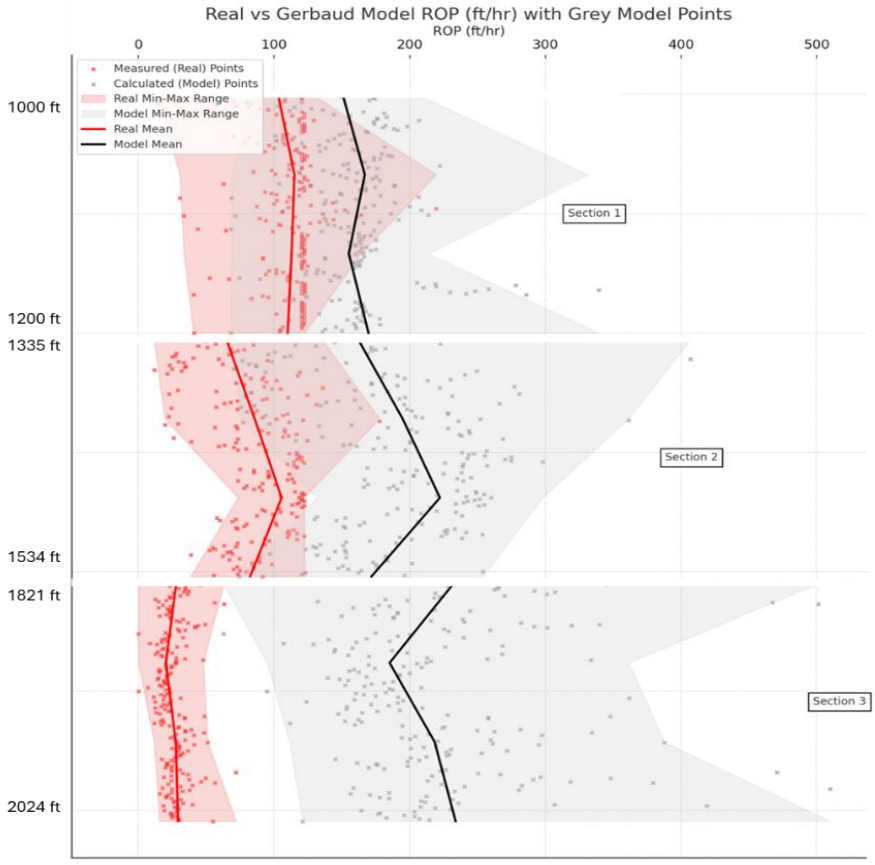

Figure 27: Real vs Gerbaud ROP model comparison

Che et al. model displayed in **Figure 28:** Real vs Che ROP model comparison shows a higher scattering for the calculated ROP, especially as the bit moves deeper. This clearly appears in sections two and three. This observation may presume that this model is more sensitive to wear compared to Detournay et al. model. A useful insight is plotted in **Figure 29:** ROP vs Wear Flat Length, where the wear flat length is plotted against the ROP. The deviation between the calculated ROPs and real ROP is seen to be increasing as the wear increases with least effect on Detournay et al. model and highest effect on Che et al. model.

Figure 28: Real vs Che ROP model comparison

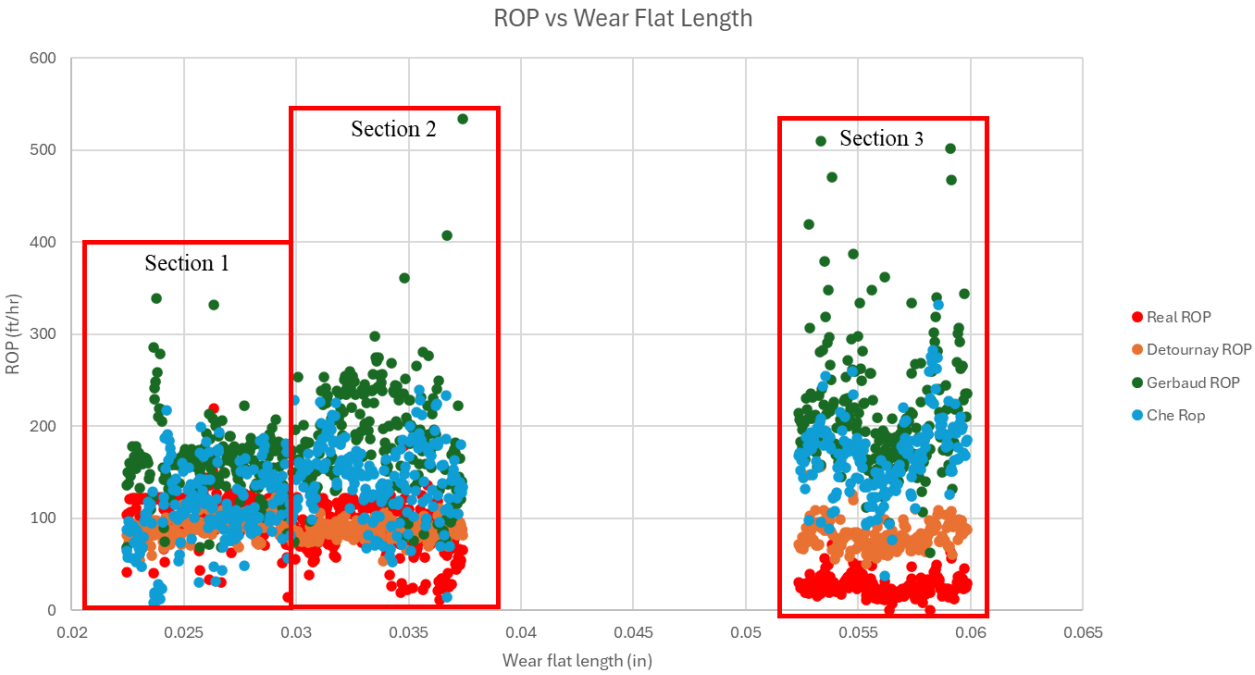

Figure 29: ROP vs Wear Flat Length

Figure 30: Different ROP models comparison is another representation of **Figure 29:** ROP vs Wear Flat Length where a comparison between all models and the real ROP is plotted showing the variations between models as the bit hits deeper depths and cutters suffer more wearing.

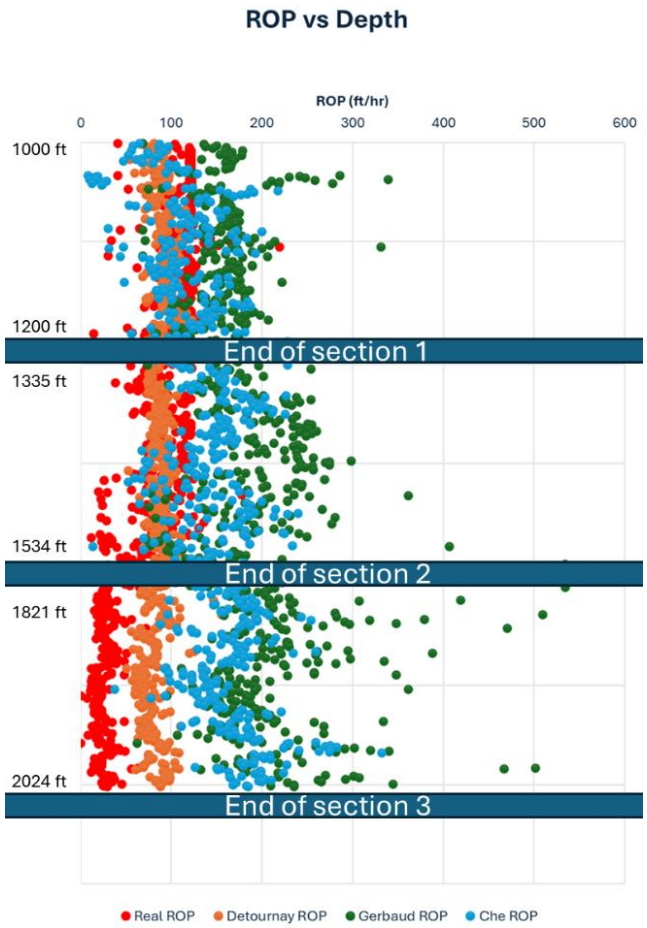

Figure 30: Different ROP models comparison

In addition to the ROP values calculated from different models, the code plots the ROP as a function in WOB and TOB as displayed in **Figure 31:** Section 1, ROP vs WOB and TOB **t**hrough **Figure 33:** Section 3, ROP vs WOB and TOBfor each section. The scattering and deviation from the real data is also sensed and obvious as the depth increases or in more specific words and the wear flat length of the cutters increases. Detournay et al. model trends are the closest to the real data behavior and in continuous decrease of ROP even with the increase of WOB and TOB due to the wearing of cutters when the bit is moving deeper. Considering the assumptions made for Gerbaud's model, the ROP was increasing with WOB and TOB in section one the ROP started to increase with TOB and decrease with WOB for sections two and three. It is noticed that Che's et al. model shows a continuous increasing trend of the ROP with both WOB and TOB.

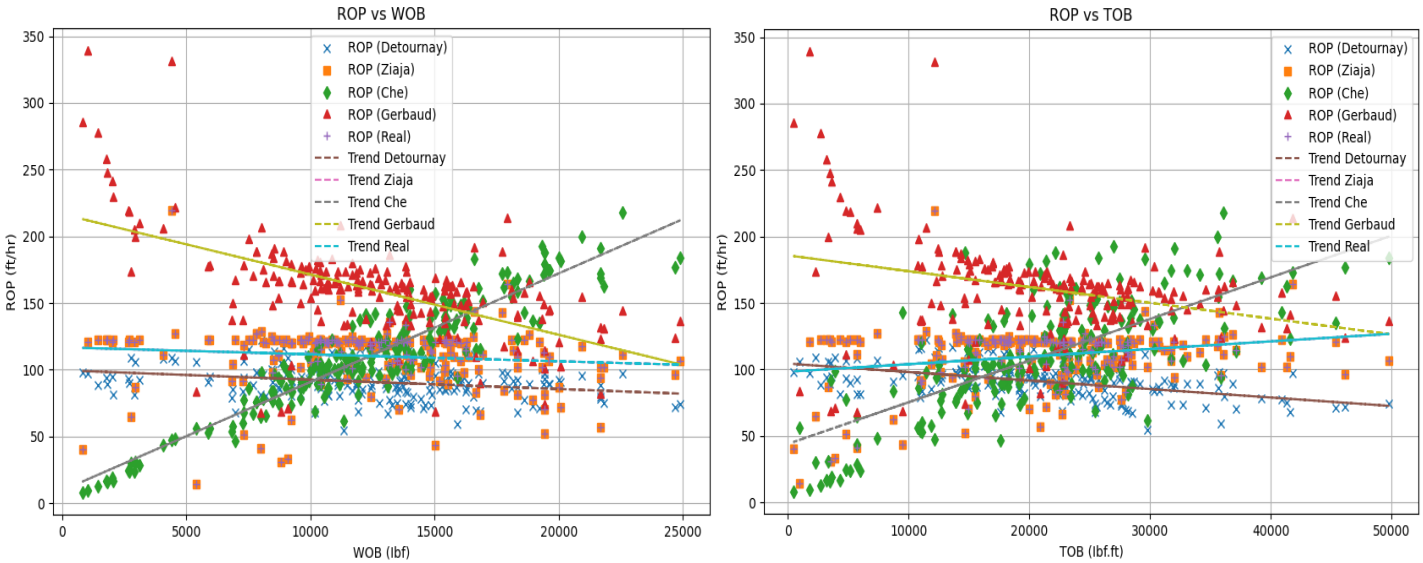

Figure 31: Section 1, ROP vs WOB and TOB

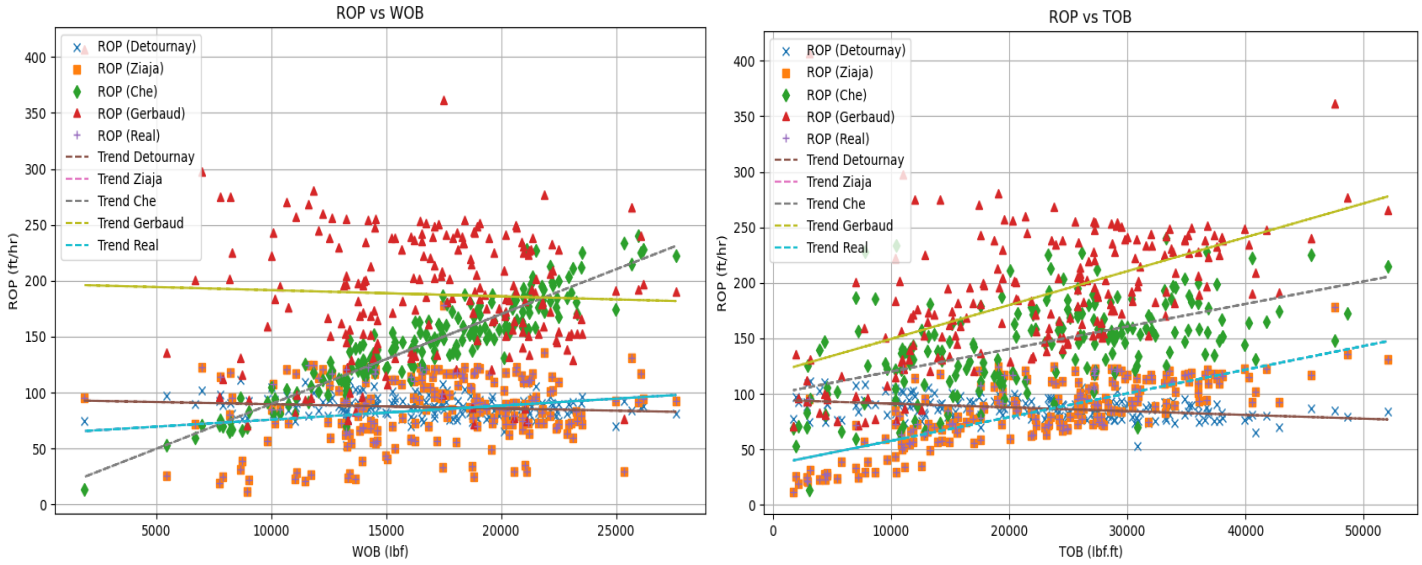

Figure 32: Section 2, ROP vs WOB and TOB

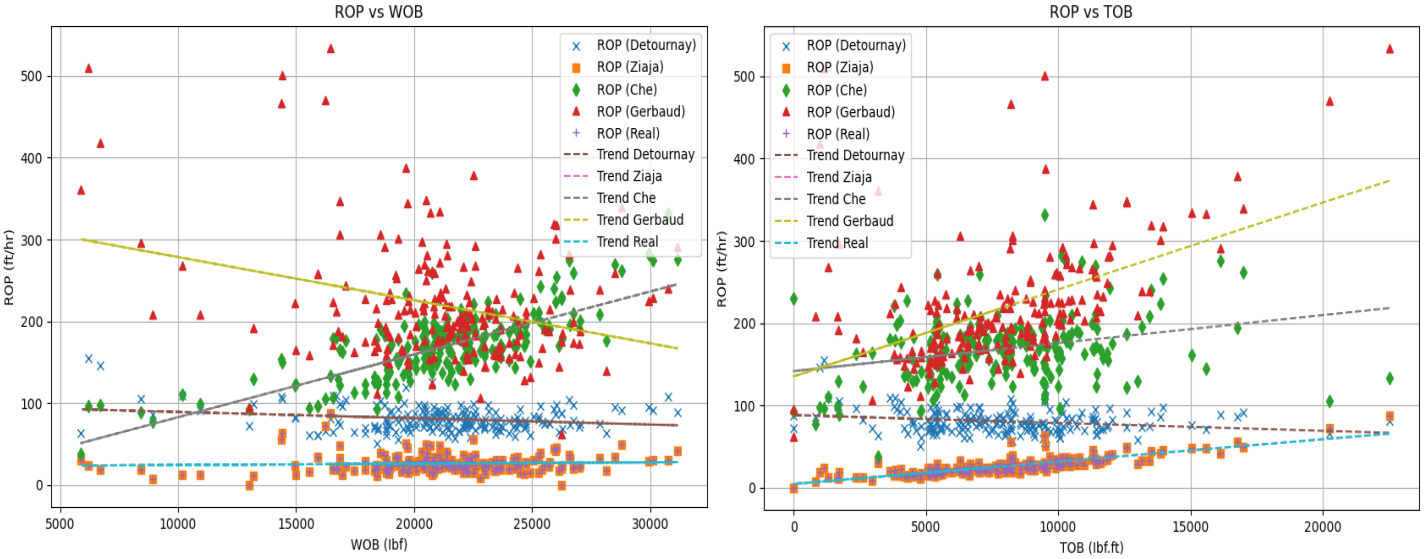

Figure 33: Section 3, ROP vs WOB and TOB

The exact match for Ziaja's model with the real data is because the depth of cut was calculated from the available data by equation 74 and not measured, which is the same equation to calculate the ROP in this model.

Conclusions

In this paper, a series of full bit and single cutter models are reviewed from literature. The presented models for PDC bit-rock interaction vary widely in complexity, assumptions, and scope. Early models like those by Ziaja, and Warren and Sinor focused on basic force resolutions and geometric relationships, introducing wear and friction considerations. Detournay et al. advanced these concepts by integrating specific energy, enabling more realistic modeling of sharp and worn cutters. Later models, such as Gerbaud's incorporated cutter shape and chamfer effects while Che et al. model considered the rock crushing in addition to shearing, capturing more nuanced rock failure mechanisms. While earlier models emphasized simplicity and field applicability, more recent work strives for comprehensive accuracy but often requires extensive data and computational resources.

A selection of these models was then implemented as a Python library. Detournay et al. and Ziaja models are a full bit models, while Gerbaud and Che et al. models are cutter models that were scaled into bit models by using the number of cutters of the used bit. The selected models are then demonstrated on a publicly available dataset from Utah FORGE. The tested models showed good agreement with the real data early in the bit life and continued to show more scattering as it drills more footage. This is related to the cutter wear effect that reduces the PDC bit performance. Detournay et al. model shows the closest ROP to the real ones. Although many assumptions were made to Gerbaud model, it shows accepted ROP calculations in the first section and gradually deviates towards the end. Che et al. model shows continuous increase in ROP and the degree of scattering as the bit drills more footage.

Acknowledgements

The authors gratefully acknowledge the support and funding of the Harold Vance Department of Petroleum Engineering and the College of Engineering at Texas A&M University and the members of the Wells for the Future Consortium.

Abbreviations

PDC		Polycrystalline diamond compact
WOB		Weight on bit
TOB		Torque on bit
ROP		Rate of penetration
RPM		Rotary speed (revolution per minute)
Glowka's empirical correlation	F	Cutter penetration force
	D	Depth of cut
	Aw	Cutter area in contact with the rock
	C	Fitting constant
	n	Fitting constant
Ziaja's model	Fvc	Vertical force
	Fhc	Horizontal force
	Rc	Index of rock strength for cutting (rock resistance)
	Rp	Index of rock strength for pressing (contact pressure)
	Sc	Cutting surface area approximated by cutter area
	α	Rake angle
	μ	Frictional factor in case of new cutter
	μ*	Frictional factor in case of worn cutter
Warren and Sinor model	Aw	Average cutter wear rate
	BR	Back rake angle
	BF	Bit factor
	C1, C2, C3 & C4	Constants
	dcm	Mean depth of cut
	dw	Width of cut
	dce	Effective depth of cut
	FN	Normal cutter force
	FV	Normal components of cutting force
	FX	Cutting force in case of friction
	RS	Relative rock strength
	a	Angle of rock internal friction
	b	Angle between bit axis and normal force
Detournay et al. model	A	Cutting cross sectional area
	ε	Rock specific energy
	ζ	Vertical to horizontal force ratio acting on the cutting face
	Fc	Force transmitted by the cutting face
	Ff	Force acting across the wear flat
	F_n^f	Vertical component of Ff
	F_s^f	Horizontal component of Ff
	μ	Coefficient of friction
	E	Specific energy
	S	Drilling strength
	a	Bit radius
	d	Depth of cut per revolution
	v	Rate of penetration
	W	Angular bit speed
	g	Bit constant
	b	Parameter characterizing drilling process and equals to $\mu\gamma\zeta$
	l	Contact length (bit wear)
	σ	Maximum normal stress that can be transmitted to the cutter
	w	Dynamic weight on bit

	t	Dynamic torque on bit
	ψ	Friction angle
	θ	Back rake angle
	k	Rate of change of contact length with the depth of cut
Wojtanowicz and Kuru model	α	Back rake angle
	αc	Cutting angle
	b	Side rake angle
	μ	Coefficient of friction
	Af	Abrasiveness constant
	Aw	Cutter wear-flat area
	Fc	Cutting force
	Ffc	Friction force acting on cutting surface area
	Ffw	Friction force effective on wear-flat area
	Fh	Horizontal force at cutter
	Fn	Normal force at cutter
	Ft	Tangential force
	Fw	Component of normal force acting on the wear-flat area
	Rc	Rock resistance to shearing
	Rp	Rock resistance to pressing
	a1	Rotary speed exponent
	db	Bit diameter
	E1 & E2	Constants calculated by integration
	I	Cutters interference constant
	N	Rotary speed
	R	Drilling rate
	h	Depth of cut
	k3	Proportionality constant between penetration rate per one rotation and cutting depth
	W	Weight on bit
Gerbaud et al. model	Fc	Forces acting on the cutting face
	Fch	Forces acting on the chamfer surface
	F^b	Forces acting on the back cutter surface
	α	Repression angle
	θ_f	Rock-cutter friction angle
	σ_0	Hydrostatic stress into the crushed zone
	ω_d	Relief angle
	ω_c	Back rake angle
	A	Cross section area of the cut
	A_{ch}	Chamfer surface area on a horizontal plane
	d	Depth of cut
	F_c	Cutting force
	F_f	Force acting upon the PDC wear flat
	R_{eq}	Rock intrinsic specific energy
Che et al. model	TCZ	Tip crushing zone
	σ_c	Rock uniaxial compressive strength
	σ_t	Rock tensile strength
	F_{TCZ}	Force acting on the TCZ
	γ	Back rake angle
	d_{TCZ}	Depth of TCZ
	w	Cutter width
	F_{pull}	Force responsible for the chipping
	α	Crack initiation angle
	d	Depth of cut
	Fc	Total cutting force
Huang et al. model	α	Back rake angle
	A	Cutter surface area
	d	Cutter diameter
	K	Drillability factor

	l	Real length of cutting arc
	l_d	Equivalent length of cutting arc
	Hd	Worn height of cutter
Atashnezhad et al. model	$\psi_{full\ bit}$	Full bit interfacial friction angle
	BG	Bit grade
	δ	Cutter depth of cut
	A_B	Bit face area
	A_v	Cutter front area
	D_c	Cutter diameter
	NOB	Number of blades
	R_e	Equivalent radius
Li et al. model	F	Resultant force on the failure line
	Fσ	Normal component of the resultant force F on the failure line
	Fτ	Tangential component of the resultant force F on the failure line
	h	Depth of cut
	n	Coefficient related to the parameters of cutting teeth
	θ	Cutting angle of the PDC cutter
	φ	Angle between direction of resultant force PL at point A and the front edge of the PDC cutter (refer to Error! Reference source not found.)
	τm	Shear strength of rock
	φk	Friction angle of rock
Wei et al. model	α	Back rake angle
	b & c	Fitting coefficients
	F_{resb}	The cutting force
	F_{basic}	Basic cutting force
	F_{chip}	Incremental cutting force
	L	Total travel length of the cutter in one cutting period
	r	Cutter diameter

References

Akbari, B., Butt, S.D., Munaswamy, K. et al. 2011. Dynamic Single PDC Cutter Rock Drilling Modeling And Simulations Focusing On Rate of Penetration Using Distinct Element Method. *Proc.*, 45th U.S. Rock Mechanics / Geomechanics Symposium, San Francisco, California.

Andersen, E. E. and Azar, J. J. 1993. PDC-Bit Performance Under Simulated Borehole Conditions. *SPE Drilling & Completion* **8** (03): SPE-20412-PA.

Atashnezhad, A., Akhtarmanesh, S., Sleeper, S. et al. 2020. Rate of Penetration (ROP) Model for PDC Drill Bits based on Cutter Rock Interaction. *Proc.*, 54th U.S. Rock Mechanics/Geomechanics Symposium, physical event cancelled.

Baird, J. A., Caskey, B. C., Wormley, D. N. et al. 1985. GEODYN2: A Bottomhole Assembly/Geological Formation Dynamic Interaction Computer Program. Las Vegas, Nevada.

Behr, S. M., Warren, T. M., Sinor, L. A. et al. 1993. 3D PDC Bit Model Predicts Higher Cutter Loads. *SPE Drilling and Completion Journal* **8** (04): 253–258.

Black, A. D., Walker, B. H., Tibbitts, G. A. et al. 1986. PDC Bit Performance for Rotary, Mud Motor, and Turbine Drilling Applications. *SPE Drilling Engineering* **1** (06): SPE-13258-PA.

Che, Demeng, Zhu, Wu-Le, and Ehmann, Kornel F. 2016. Chipping and crushing mechanisms in orthogonal rock cutting. *International Journal of Mechanical Sciences* **119**: 224-236.

Chen, S., Collins, G. J., and Thomas, M. B. 2008. Reexamination of PDC Bit Walk in Directional and Horizontal Wells. *Proc.*, IADC/SPE Drilling Conference, Florida.

Detournay, E. and Defourny, P. 1992. A phenomenological model for the drilling action of drag bits. *International Journal of Rock Mechanics and Mining Sciences & Geomechanics Abstracts* **29** (1): 13-23.

Detournay, Emmanuel, Richard, Thomas, and Shepherd, Mike. 2008. Drilling response of drag bits: Theory and experiment. *International Journal of Rock Mechanics and Mining Sciences* **45** (08): 1347-1360.

Endres, Lanson Adam. 2007. Computation modeling of drill bits : a new method for reproducing bottom hole geometry and a second-order explicit integrator via composition for coupled rotating rigid bodies. Doctor of Philosophy Dissertation, UNIVERSITY OF CALIFORNIA SAN DIEGO.

Feenstra, R. 1988. Status of Polycrystalline-Diamond-Compact Bits. *Journal of Petroleum Technology* **40** (06): SPE-17919-PA.

Gerbaud, L., Menand, S., and Sellami, H. 2006. PDC Bits: All Comes from the Cutter/Rock Interaction. *Proc.*, IADC/SPE Drilling Conference, Florida.

Geothermal Data Repository. 2023. *Utah FORGE: Logs and Data from Deep Well 58-32* (Reprint). https://gdr.openei.org/submissions/1006.

Glowka, David A. 1989. Use of Single-Cutter Data in the Analysis of PDC Bit Designs: Part 1 - Development of a PDC Cutting Force Model *Journal of Petroleum Technology* **41** (08): 798-799 & 844-849.

Hanson, J. M. and Hansen, W. R. 1995. Dynamics Modeling of PDC Bits *Proc.*, SPE/IADC Drilling Conference, Amsterdam, Netherlands.

Huang, Hsin I. and Iversen, Robert E. 1981. The Positive Effects of Side Rake in Oilfield Bits Using Polycrystalline Diamond Compact Cutters. *Proc.*, SPE Annual Technical Conference and Exhibition, San Antonio.

Huang, Jian, Zeng, Bo, He, Yuhang et al. 2023. Numerical study of rock-breaking mechanism in hard rock with full PDC bit model in compound impact drilling. *Energy Reports* **9**: 3896-3909.

Huang, Zhiqiang, Ma, Yachao, Li, Qin et al. 2017. Geometry and force modeling, and mechanical properties study of polycrystalline diamond compact bit under wearing condition based on numerical analysis. *Advances in Mechanical Engineering* **9** (6).

Langeveld, C. J. 1992. PDC Bit Dynamics. *Proc.*, IADC/SPE Drilling Conference, New Orleans, Louisiana.

Li, Wei, Ling, Xin, and Pu, Hui. 2020. Development of a Cutting Force Model for a Single PDC Cutter Based on the Rock Stress State. *Rock Mechanics and Rock Engineering* **53**: 185-200.

Mat, M. Rujhan, Zakaria, Mohd Zulkifi Bin, Radford, Steve et al. 2002. Innovative Low-Friction Coating Reduces PDC Balling and Doubles ROP Drilling Shales with WBM *Proc.*, IADC/SPE Drilling Conference, Dallas.

Mensa-Wilmot, Graham and Penrose, Bill. 2003. Advanced Cutting Structure Improves PDC Bit Performance in Hard and Abrasive Drilling Environments. *Proc.*, SPE Latin American and Caribbean Petroleum Engineering Conference, Port-of-Spain, Trinidad and Tobago.

Millheim, K.K. 1986. Advances in Drilling Technology (1981-1986) and Where Drilling Technology Is Heading. *Proc.*, International Meeting on Petroleum Engineering, Beijing.

Offenbacher, L. A., McDermaid, J. D., and Patterson, C. R. 1983. PDC Bits Find Applications in Oklahoma Drilling. *SPE Drilling Engineering*: SPE-11389-MS.

Paterson, A. and Suute, J. 1982. Experience with Polycrystalline Diamond Compact Bits in the Northern North Sea. *Proc.*, European Petroleum Conference, London.

Pelfrene, Gilles, Stab, Olivier, Tilleman, Danny et al. 2019. Modelling the 3D Bit-Rock Interaction Helps Designing Better PDC Bits *Proc.*, SPE/IADC International Drilling Conference and Exhibition, The Netherlands.

Powell, R., Cooke, G., and Hippmann, A. 1980. The Versatility of the Turbodrill in North Sea Drilling. *Proc.*, European Offshore Petroleum Conference, London.

Prooyen, J., Juergen, R., and Gilbert, H. 1982. "Recent Results with New Bits. *Proc.*, SPE Middle East Oil Technical Conference, Bahrain.

Pryhorovska, T. O., Chaplinskiy, S. S., and Kudriavtsev, I. O. 2015. Finite element modelling of rock mass cutting by cutters for PDC drill bits. *Petroleum Exploration and Development* **42** (06): 888-892.

Radford, S.R.. R., Patel, S.G.. G., and Dee, K.C.. C. 2015. Durable Bit Coating Reduces Shale Balling in Field Tests and Contributes to Longer Runs. *Proc.*, SPE/IADC Drilling Conference and Exhibition, London.

Radtke, Robert P., Riedel, Richard, and Hanaway, John. 2004. Thermally Stable Polycrystalline Diamond Cutters for Drill Bits. *Proc.*, SPE Annual Technical Conference and Exhibition, Houston.

Shor, Roman J., Kandala, Shanti Swaroop, Gildin, Eduardo et al. 2022. Progress Toward an Open-Source Drilling Community: Contributing and Curating Models. *Proc.*, IADC/SPE International Drilling Conference and Exhibition, Galveston, Texas, USA.

Smith, R. H., Lund, J. B., Anderson, M. et al. 1995. Drilling Plastic Formations Using Highly Polished PDC Cutters. *Proc.*, SPE Annual Technical Conference and Exhibition, Dallas.

Sneddon, M.V. and Hall, D.R. 1988. Polycrystalline Diamond: Manufacture, Wear Mechanisms, and Implications for Bit Design. *Journal of Petroleum Technology* **40** (12): SPE-17006-PA.

Spencer, Reed, Hanson, Jonathan, Hoffmann, Olivier et al. 2013. New Directional Drilling Simulation Tool Reveals Link between Dynamic Stability and Tool Face Control. *Proc.*, SPE/IADC Drilling Conference, Amsterdam, The Netherlands.

University of Utah. 2023 (Reprint). https://utahforge.com/about-us/?utm_source.

Warren, T. M. and Armagost, W. K. 1988. Laboratory Drilling Performance of PDC Bits. *SPE Drilling Engineering* **3** (02): SPE-15617-PA.

Warren, T. M. and Sinor, A. 1986. Drag-Bit Performance Modeling. *SPE Drilling Engineering* **4** (02): 119-127.

Wei, Jiusen, Liu, Wei, and Gao, Deli. 2024a. Mechanism Analysis and Mathematical Modeling of Brittle Failure in Rock Cutting with a Single Sharp Cylinder-Shaped PDC Cutter. *SPE Journal* **29** (02): 651–669.

Wei, Jiusen, Liu, Wei, and Gao, Deli. 2024b. Modeling of PDC bit-rock interaction behaviors based on the analysis of dynamic rock-cutting process. *Geoenergy Science and Engineering* **239**.

Wojtanowicz, A. K. and Kuru, E. 1993. Mathematical Modeling of PDC Bit Drilling Process Based on a Single-Cutter Mechanics. *J Energy Resour Technol* **115** (4): 247-256.

Yari, Nina, Kapitaniak, Marcin, Vaziri, Vahid et al. 2018. Calibrated FEM modelling of rock cutting with PDC cutter. *Proc.*, International Conference on Engineering Vibration, Sofia, Bulgaria.

Yazidi, A.. 2013. Exploiting the Latent Benefits of Wired Pipes: A Comprehensive Decision Making System. *Proc.*, SPE Digital Energy Conference, The Woodlands.

Zhan, Guodong David, Moellendick, Timothy Eric, Li, Bodong et al. 2020. New Ultra-Strong and Catalyst-Free PDC Cutting Element Technology. *Proc.*, International Petroleum Technology Conference, Dhahran.

Ziaja, M. B. 1985. Mathematical Model of the Polycrystalline Diamond Bit Drilling Process and Its Practical Application. *Proc.*, SPE Annual Technical Conference and Exhibition, Las Vegas, Nevada.